2003

Steady state free radical budgets and ozone photochemistry during TOPSE

Christopher A. Cantrell

L. Mauldin

See next page for additional authors

Citation/Publisher Attribution

Cantrell, C. A., et al. (2003), Steady state free radical budgets and ozone photochemistry during TOPSE, *J. Geophys. Res.*, 108, 8361, doi: 10.1029/2002JD002198, D4.
Available at: https://doi.org/10.1029/2002JD002198

Authors
Christopher A. Cantrell, L. Mauldin, M. Zondlo, F. Eisele, E. Kosciuch, R. Shetter, B. Lefer, S. Hall, T. Campos, B. Ridley, J. Walega, A. Fried, B. Wert, F. Flocke, A. Weinheimer, J. Hannigan, M. Coffey, E. Atlas, S. Stephens, Brian G. Heikes, J. Snow, D. Blake, N. Blake, A. Katzenstein, J. Lopez, E. V. Browell, J. Dibb, E. Scheuer, G. Seid, and R. Talbot

Steady state free radical budgets and ozone photochemistry during TOPSE

Christopher A. Cantrell,[1] L. Mauldin,[1] M. Zondlo,[1] F. Eisele,[1,2] E. Kosciuch,[1] R. Shetter,[1] B. Lefer,[1] S. Hall,[1] T. Campos,[1] B. Ridley,[1] J. Walega,[1] A. Fried,[1] B. Wert,[1] F. Flocke,[1] A. Weinheimer,[1] J. Hannigan,[1] M. Coffey,[1] E. Atlas,[1] S. Stephens,[1] B. Heikes,[3] J. Snow,[3] D. Blake,[4] N. Blake,[4] A. Katzenstein,[4] J. Lopez,[4] E. V. Browell,[5] J. Dibb,[6] E. Scheuer,[6] G. Seid,[6] and R. Talbot[6]

Received 12 February 2002; revised 2 May 2002; accepted 21 June 2002; published 5 February 2003.

[1] A steady state model, constrained by a number of measured quantities, was used to derive peroxy radical levels for the conditions of the Tropospheric Ozone Production about the Spring Equinox (TOPSE) campaign. The analysis is made using data collected aboard the NCAR/NSF C-130 aircraft from February through May 2000 at latitudes from 40° to 85°N, and at altitudes from the surface to 7.6 km. HO_2 + RO_2 radical concentrations were measured during the experiment, which are compared with model results over the domain of the study showing good agreement on the average. Average measurement/model ratios are 1.04 (σ = 0.73) and 0.96 (σ = 0.52) for the MLB and HLB, respectively. Budgets of total peroxy radical levels as well as of individual free radical members were constructed, which reveal interesting differences compared to studies at lower latitudes. The midlatitude part of the study region is a significant net source of ozone, while the high latitudes constitute a small net sink leading to the hypothesis that transport from the middle latitudes can explain the observed increase in ozone in the high latitudes. Radical reservoir species concentrations are modeled and compared with the observations. For most conditions, the model does a good job of reproducing the formaldehyde observations, but the peroxide observations are significantly less than steady state for this study. Photostationary state (PSS) derived total peroxy radical levels and NO/NO_2 ratios are compared with the measurements and the model; PSS-derived results are higher than observations or the steady state model at low NO concentrations. *INDEX TERMS:* 0365 Atmospheric Composition and Structure: Troposphere—composition and chemistry; 0368 Atmospheric Composition and Structure: Troposphere—constituent transport and chemistry; 0317 Atmospheric Composition and Structure: Chemical kinetic and photochemical properties; 0345 Atmospheric Composition and Structure: Pollution—urban and regional (0305)

Citation: Cantrell, C. A., et al., Steady state free radical budgets and ozone photochemistry during TOPSE, *J. Geophys. Res.*, *108*(D4), 8361, doi:10.1029/2002JD002198, 2003.

1. Introduction

[2] The free radical chemistry of the troposphere has been a subject of scientific interest and investigation for several decades [*Levy*, 1971; *Crutzen*, 1971], and has undergone renewed scrutiny as reliable in situ measurements have been reported in the last 10 years or so [e.g., *Mount*, 1992; *Brune et al.*, 1995; *Cantrell et al.*, 1996a, 1997b, 2003; *Wennberg et al.*, 1998; *Holland et al.*, 1998; *Mauldin et al.*, 1999; *Reiner et al.*, 1999; *Burkert et al.*, 2001; *Creasey et al.*, 2001; *Kanaya et al.*, 2001]. Much has been learned regarding the sources of HO_x (= OH + HO_2) and RO_2 throughout the troposphere. New sources of radicals in the upper troposphere have been proposed and investigated, and the role of convection in transporting radical precursors has been studied [e.g., *Lelieveld and Crutzen*, 1994; *Singh et al.*, 1994; *Jaeglé et al.*, 1997, 2001; *McKeen et al.*, 1997; *Prather and Jacob*, 1997; *Wennberg et al.*, 1998; *Cohan et al.*, 1999; *Wang and Prinn*, 2000]. The comparison of measurements of free radical concentrations with constrained models has led to improved understanding and uncovered gaps in mechanisms of free radical production, conversion and loss.

[1]Atmospheric Chemistry Division, National Center for Atmospheric Research, Boulder, Colorado, USA.
[2]Georgia Institute of Technology, Atlanta, Georgia, USA.
[3]School of Oceanography, University of Rhode Island, Narragansett, Rhode Island, USA.
[4]University of California-Irvine, Irvine, California, USA.
[5]Atmospheric Sciences, NASA Langley Research Center, Hampton, Virginia, USA.
[6]University of New Hampshire, Durham, New Hampshire, USA.

0148-0227/03/2002JD002198

[3] The Tropospheric Ozone Production about the Spring Equinox (TOPSE) program was planned to examine the evolution of photochemistry and transport at northern middle to high latitudes during the winter-to-spring seasonal transition particularly as these processes relate to the seasonal increase in ozone concentrations that has been observed in the middle troposphere (E. Atlas, B. Ridley, and C. Cantrell, The Tropospheric Ocean Production about the Spring Equinox (TOPSE) Experiment: Introduction, submitted to *Journal of Geophysical Research*, 2003, hereinafter referred to as Atlas et al., submitted manuscript, 2003). A component of this program was the C-130 aircraft operated by NCAR and the National Science Foundation. It was configured with a suite of instruments employed to measure components related to the ozone photochemical budget, and to determine the abundance of tracers of air mass origin in the stratosphere or the boundary layer. In addition, an enhanced ozonesonde network was deployed (J. Merrill, personal communication), and collaboration was established with a ground-based measurement campaign at Alert, Nunavut, Canada [e.g., *Hopper et al.*, 1998], part of a series of experiments performed since the 1980s. Aircraft flights were conducted in seven deployments from early February to mid-May, with flights from Jefferson County Airport (in the Denver, Colorado, USA suburban area) to Winnipeg, Manitoba, Canada, to Churchill, Manitoba, to Thule, Greenland, and north. Latitudes from 39.85 to 85.12°N, and altitudes from the surface to 7.6 km were sampled.

[4] One of the instruments on the aircraft platform was a 4-channel chemical ionization mass spectrometer (CIMS) system [*Mauldin et al.*, 2003]. This instrument has been deployed in other aircraft missions including PEM-Tropics B [*Mauldin et al.*, 2002]. It is composed of a common vacuum system containing the mass spectrometer components to which a variety of inlets with differing neutral and ion chemistries can be attached. For the TOPSE mission, there was a channel for the measurement of OH, H_2SO_4 and MSA (methane sulfonic acid) [*Mauldin et al.*, 2003] a channel dedicated to the determination of HNO_3 concentrations (M. A. Zondlo et al., Development and characterization of an airborne-based instrument used to measure nitric acid during the NASA TRACE-p field experiment, submitted to *Journal of Geophysical Research*, 2003), and one for measurement of HO_2 and RO_2 radicals [*Cantrell et al.*, 2003]. Atlas et al. (submitted manuscript, 2003) provide a full description of the aircraft-based instrumentation deployed during TOPSE; species and parameters measured included CO, N_2O, CH_4, j-values, CH_2O, peroxides, NO_x, PAN, PPN thermally labile PANs, alkyl nitrates, NO_y, O_3 (in situ and remote via DIAL), nonmethane hydrocarbons, chlorinated hydrocarbons, soluble acidic gases, aerosols (in situ and remote), in addition to the radicals and sulfur gases listed above.

[5] For the purposes of this discussion, the following families are defined. HO_x is the sum of the OH and HO_2 concentrations, HO_xRO_x is defined to be the sum of HO_x and RO_2, where R is any organic group, and HO_y is the sum of HO_xRO_x and the radical reservoirs, namely $(2 \times H_2O_2) + (2 \times CH_3OOH) + PAN + HONO + CH_3O_2NO_2 + HO_2NO_2$ (coefficients indicate number of radicals produced from photolysis).

[6] Peroxy radicals are produced in the troposphere through a variety of photolytic and thermal processes. Reactions that convert radicals within the HO_xRO_x family are usually rapid, and thus sources of OH, HO_2 and RO_2 contribute to this free radical family. This includes the photolysis of ozone in the ultraviolet-B spectral region ($\leq$340 nm), followed by reaction of the $O(^1D)$ product with water vapor, which initially produces OH. $O(^1D)$ may also be quenched to ground-state oxygen atoms.

$$O_3 + h\nu \rightarrow O(^1D) + O_2 \quad (1)$$

$$O(^1D) + M \rightarrow O(^3P) + M \quad (2)$$

$$O(^1D) + H_2O \rightarrow 2OH \quad (3)$$

[7] Other photolytic processes, such as formaldehyde photolysis also produce radicals; photolysis of formaldehyde can also produce H_2 and CO.

$$CH_2O + h\nu \rightarrow H + HCO \quad (4)$$

[8] In the troposphere, the atom and radical fragments, H and HCO, rapidly react with molecular oxygen to produce HO_2.

[9] Radicals are destroyed through radical-radical and radical-NO_2 reactions. The reactions between radicals include the disproportionation reaction of HO_2, which has bimolecular and termolecular channels that are enhanced by water vapor [see, e.g., *Stockwell*, 1995, and references therein].

$$HO_2 + HO_2(M, H_2O) \rightarrow H_2O_2 + O_2 \quad (5)$$

[10] Reaction between HO_2 and RO_2 (including CH_3O_2) produces hydroperoxides and other products, depending on the structure of the "R" group. There is evidence from laboratory studies [*Elrod et al.*, 2001] that a channel in this reaction could exist leading to the production of an aldehyde (CH_2O in the reaction of HO_2 with CH_3O_2) (reaction (16)).

$$HO_2 + RO_2 \rightarrow ROOH + O_2 \quad (6a)$$

$$\rightarrow R'COOH + O_3 \quad (6b)$$

$$\rightarrow R'CHO + H_2O + O_2 \quad (6c)$$

Many important tropospheric reactions involve the interconversion of radicals between OH, HO_2 and RO_2. Organic compounds are attacked by OH leading to HO_2 or RO_2 radicals

$$OH + RH(O_2, M) \rightarrow H_2O + RO_2 \quad (7)$$

[11] HO_2 and RO_2 react with NO to produce NO_2 and other HO_xRO_x radicals (including HO_2 or other RO_2 radicals).

$$HO_2 + NO \rightarrow OH + NO_2 \quad (8)$$

$$RO_2 + NO \rightarrow RO + NO_2 \quad (9a)$$

$$RO + O_2 \rightarrow R'CHO + HO_2 \quad (10)$$

[12] Alkyl peroxy radicals also react with NO in a branch leading to a loss of HO_xRO_x (in addition to a conversion reaction (9a)). The fraction k_{9b}/k_9 (where k_9 is the sum of k_{9a} and k_{9b}) depends on the nature of the R group; the importance generally increases with the carbon number of the R group [*Atkinson*, 1994].

$$RO_2 + NO + M \rightarrow RONO_2 + M \qquad (9b)$$

Depending on the structure of the RO radicals produced in reaction (9a), isomerization and/or decomposition could compete with reaction (10) to lead to fragments that produce other RO_2 radicals.

[13] Direct measurements of members of the HO_xRO_x family can provide tests of our understanding of tropospheric free radical chemistry. These are aided by measurements of the controlling species and reaction rate coefficients (including photolysis rate coefficients). From these latter measurements, radical budgets can be constructed. The HO_xRO_x and OH measurements are presented in detail elsewhere [*Cantrell et al.*, 2003] [*Mauldin et al.*, 2003]. Thus, the goal of this paper is to make use of a constrained steady state model to examine the free radical amounts and rates of key reactions in order to gain understanding of the factors that control the trends of photochemical activity in the study region during the winter-to-spring seasonal transition. Specifically, we will attempt to ascertain (1) differences in components of HO_xRO_x budgets between middle and high latitudes and the changes that occur with season, (2) a general picture of the role of free radicals in the source and sink terms of the ozone budget, (3) the ability of the photostationary state assumption to reproduce the HO_xRO_x levels and NO/NO_2 ratios, and (4) the degree of agreement between peroxide and formaldehyde measurements and that expected from free radical chemistry, and the implications of these comparisons. The companion papers by *Fried et al.* [2003] will present such comparisons for CH_2O in more detail, and the peroxide results are examined by *Snow et al.* [2003]. The comparisons between OH measurements and the results of the present steady state model are discussed in *Mauldin et al.*, [2003].

2. Observations and Models

2.1. Peroxy Radical Measurements

[14] Peroxy radicals were measured during TOPSE using the PerCIMS technique based on the chemical conversion of HO_2 and RO_2 into H_2SO_4, chemical ionization, and mass spectrometric detection [*Eisele et al.*, 1996; *Cantrell et al.*, 1997b, 2003; *Reiner et al.*, 1999]. The measurement technique is described in detail elsewhere (G. D. Edwards et al., A chemical ionization mass spectrometer instrument for the measurement of tropospheric HO_2 and RO_2, in preparation for *Analytical Chemistry*, 2003), as are the TOPSE measured peroxy radical concentrations [*Cantrell et al.*, 2003] and the TOPSE measured OH concentrations [*Mauldin et al.*, 2003]. The basis of the peroxy radical measurements is the chemical conversion of radicals into gas-phase sulfuric acid (H_2SO_4) followed by chemi-ionization through reaction with NO_3^-. The chemical conversion takes place by the addition of NO and SO_2 to the instrument inlet. Reagent ions are produced by passing gas-phase nitric acid (HNO_3) over a radioactive Americium-241 source. The reagent and product ions are detected by selected ion mass spectrometry that includes several stages of differential pumping, mass filtering, and ion counting. Calibrations are performed using the quantitative photolysis of water vapor at 184.9 nm; a linear relationship exists between the HSO_4^-/NO_3^- ion ratio and the peroxy radical concentration. Radical concentrations (HO_xRO_x and HO_2) can be quantified with an estimated accuracy of ±35% at levels much greater than the detection limit. Typical lower limits of detection were 1×10^7 radicals-cm^{-3} in 1 minute, but were sometimes poorer due to degraded instrument performance from shorting of ion-directing lenses within the instrument inlet. Since average levels observed were in the low 10^8 cm^{-3} range, signal to noise ratios typically were greater than 10 for one-minute average results.

[15] A summary of measured HO_xRO_x concentrations is presented in Figure 1, in which panel (a) shows a smoothed altitude-time profile for latitudes of 40–60 degrees north (midlatitude band, MLB), and panel (b) corresponds to measurements made at 60–85 degrees north (high latitude band, HLB). These latitude bands were selected using Churchill as an approximate separation point. The smoothing was performed using the SigmaPlot 2001 program (SPSS Inc.) which entailed generating a 25 by 25 data point matrix for each plot. Each point in the matrix is calculated from the weighted average of the nearest 10% of the raw data using the Cauchy density function. Note that the entire time and space (latitude-altitude) domain was not sampled (see Atlas et al., submitted manuscript, 2003). Studies took place on days 35–40, 52–58, 65–68, 79–86, 93–102, 114–121 and 136–144 (groups of days represent each of the seven deployments) and peroxy radical measurements were performed for a fraction of the time available. The details of the measurement altitude and time coverage are discussed in *Cantrell et al.* [2003]. Data availability was good in the MLB except at altitudes greater that 6 km in the first deployment, at middle and lower altitudes during the third deployment, and at all altitudes during the fifth deployment; in the HLB, there was less data in the first three deployments at altitudes greater than 6 km, and from 1 to 4 km during the first, second, third and fifth deployments. For these locations and times described, there were less than 10 data points per bin, where the bins are defined as 1 km altitudes within a given deployment. Thus, the measurement-model comparisons during these periods are less meaningful than during the rest of the study. On the average, there are 20 to 40 measured points per altitude-deployment bin for the MLB, and 15 to 35 points per bin for the HLB. The averages are 50 and 75 points, respectively for the seventh deployment. The average numbers of steady state modeling points per bin are 85 to 110 for MLB, and 80 to 120 for the HLB. In the HLB on deployments 1 and 3, there are fewer points; the averages are 37 and 28 points per bin, respectively. Differences between the observations and the surfaces presented in Figure 1 were calculated. In the MLB, the absolute deviations of the observations from the surface average 34% (σ = 26%); absolute deviations for the HLB average 50% (σ = 35%). Deviations for the steady state model surfaces are similar, with the model deviations somewhat smaller than those for the measurements in the HLB.

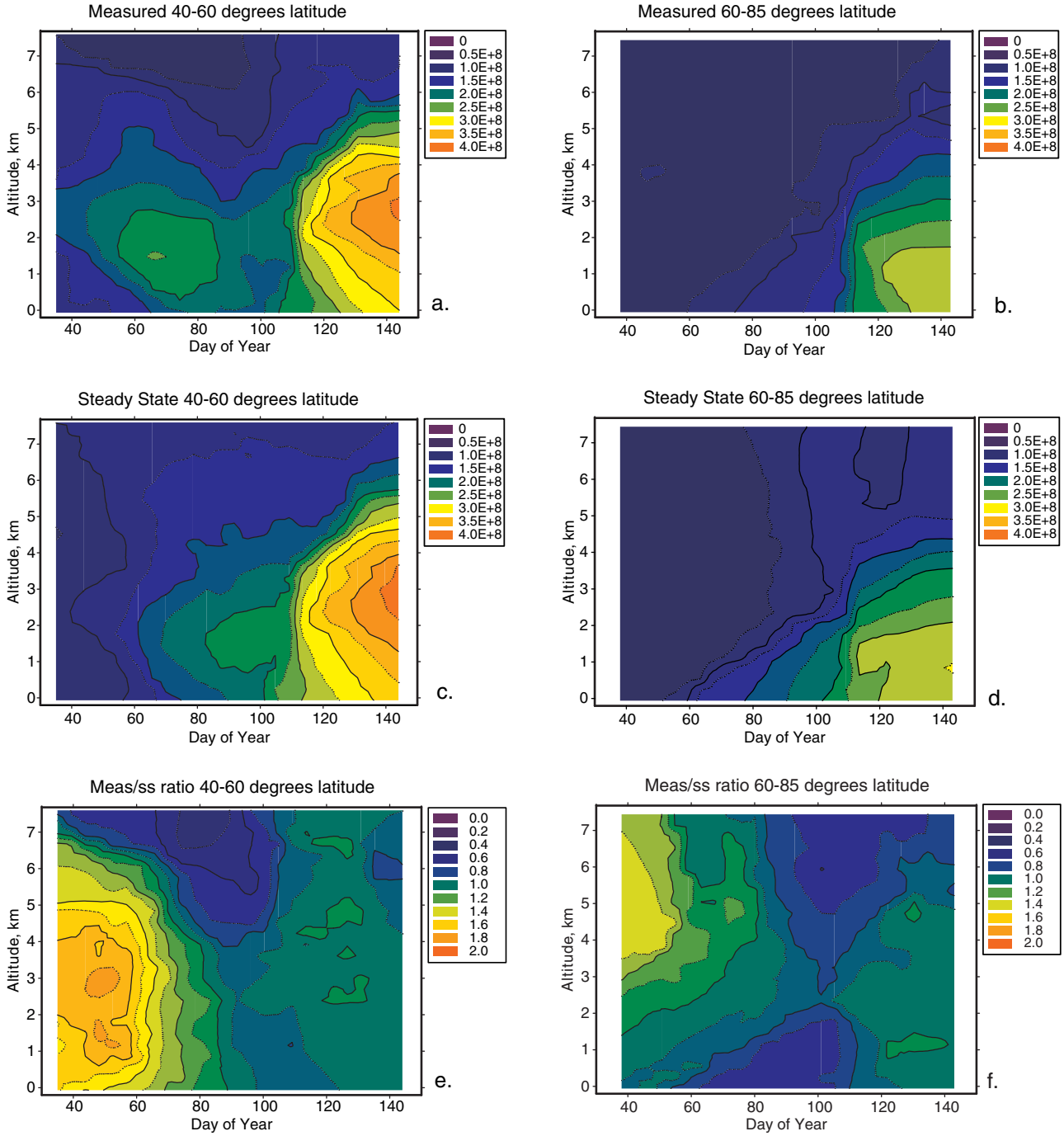

Figure 1. TOPSE peroxy radical concentrations (a, b) measured, (c, d) calculated from steady state model at the coincident measurements, and (e, f) ratio of coincident measured to steady state concentrations, for the MLB (left) and HLB (right) regions.

[16] Of the 12,103 one-minute time periods for which data could be potentially collected, measured HO_xRO_x concentrations are available for 3599 of them (about 30% coverage), and HO_2 concentrations are available for a very small fraction, in this first aircraft deployment. This compares with data coverage percentages of 94, 82, 72, 55, 42, 35, and 17% for jNO_2, O_3, NO_x, SO_2, CH_2O, propane, and OH, respectively. Data coverage is reduced because of calibrations and other instrumental maintenance, breakdowns, and also, in the case of the CIMS instrument, shutdown during takeoff and landing. More details on the data, including dependence on various variables are available in *Cantrell et al.* [2003].

[17] It can be seen that peroxy radical levels increase with altitude to peak concentrations between 1 and 3 km and decrease at higher altitudes, increase with day of year, and, for a given altitude and day of year, the levels are lower at higher latitudes. In fact, it appears that the radical levels at the higher latitude band lag those at the lower latitude band by about 20–30 days. One can envision a "bloom" in

Table 1. Chemical Mechanism Used for Steady State Calculations

Reaction	Rate Coefficient	
$O_3 + h\nu \rightarrow O(^1D) + O_2$	Variable	
$NO_2 + h\nu \rightarrow O(^3P) + NO$	Variable	
$CH_2O + h\nu \rightarrow H + HCO$	Variable	
$CH_2O + h\nu \rightarrow H_2 + CO$	Variable	
$H_2O_2 + h\nu \rightarrow 2\ OH$	Variable	
$CH_3OOH + h\nu \rightarrow CH_3O + OH$	Variable	
$(CH_3)_2CO + h\nu \rightarrow CH_3 + CH_3CO$	Variable	
$HO_2NO_2 + h\nu \rightarrow HO_2 + NO_2$	Variable	
$HO_2NO_2 + h\nu \rightarrow OH + NO_3$	Variable	
$CH_3O_2NO_2 + h\nu \rightarrow CH_3O_2 + NO_2$	Variable	
$CH_3O_2NO_2 + h\nu \rightarrow CH_2O + NO_3$	Variable	
$PAN + h\nu \rightarrow CH_3C(O)O_2 + NO_2$	Variable	
$O(^1D) + H_2O \rightarrow 2\ OH$	2.2E−10,0	D
$O(^1D) + N_2 \rightarrow O(^3P) + N_2$	1.8E−11,−110	D
$O(^1D) + O_2 \rightarrow O(^3P) + O_2$	3.2E−11,−70	D
$O(^3P) + O_2 + M \rightarrow O_3 + M$	Fast	
$H + O_2 + M \rightarrow HO_2 + M$	Fast	
$HCO + O_2 \rightarrow HO_2 + CO$	Fast	
$CH_3O + O_2 \rightarrow CH_2O + HO_2$	Fast	
$CH_3 + O_2 + M \rightarrow CH_3O_2 + M$	Fast	
$R + O_2 + M \rightarrow RO_2 + M$	Fast	
$HO_2 + O_3 \rightarrow OH + 2\ O_2$	1.1E−14,500	D
$OH + O_3 \rightarrow HO_2 + O_2$	1.6E−12,940	D
$HO_2 + HO_2\ (M,H_2O) \rightarrow H_2O_2 + O_2$	(2.3E−13,−600 + 1.7E−33 × M, −1000) × (1 + 1.4E−21 × H_2O,−2200)	D
$HO_2 + CH_3O_2 \rightarrow CH_3OOH + O_2$	3.8E−13,−800	A2
$HO_2 + CH_3O_2 \rightarrow CH_2O + H_2O + O_2$	1.6E−15,−1730	E
$HO_2 + RO_2 \rightarrow ROOH + O_2$	3.5E−13,−1000	A4
$CH_3O_2 + CH_3O_2 \rightarrow 2\ CH_3O + O_2$	5.94E−13,505	A4
$CH_3O_2 + CH_3O_2 \rightarrow CH_3OH + CH_2O + O_2$	1.1E−13,−365 × (1−5.4,870)	A4
$RO_2 + RO_2 \rightarrow 2\ RO + O_2$	5.94E−13,505	A4
$RO_2 + RO_2 \rightarrow ROH + R'CHO + O_2$	1.1E−13,−365 × (1−5.4,870)	A4
$HO_2 + OH \rightarrow H_2O + O_2$	4.8E−11,−250	D
$OH + H_2O_2 \rightarrow H_2O + HO_2$	2.9E−12,160	D
$O_3 + NO \rightarrow NO_2 + O_2$	2.0E−12,1400	D
$HO_2 + NO \rightarrow OH + NO_2$	3.7E−12,−240	A92
$CH_3O_2 + NO \rightarrow CH_3O + NO_2$	4.2E−12,−180	A92
$RO_2 + NO \rightarrow RO + NO_2$	4.9E−12,−180	A94
$HO_2 + NO_2 + M \rightarrow HO_2NO_2 + M$	k_o: 1.8E−31$(T/300)^{-3.2}$; k_8: 4.7E−12$(T/300)^{-1.4}$	D
$HO_2NO_2 + M \rightarrow HO_2 + NO_2 + M$	K_{eq}: 2.1E−27,−10900	D
$OH + NO_2 + M \rightarrow HNO_3 + M$	k_o: 2.5E−30$(T/300)^{-4.4}$; k_8: 1.6E−11$(T/300)^{-1.7}$	D
$OH + HNO_3 \rightarrow H_2O + NO_3$	k_o: 7.2E−15,−785; k_2: 4.1E−16,−1440; k_3: 1.9E−33,−725	D
$OH + HO_2NO_2 \rightarrow H_2O + NO_2 + O_2$	1.3E−12,−380	D
$OH + NO + M \rightarrow HONO + M$	k_o: 7.0E−31$(T/300)^{-2.6}$; k_8: 3.6E−11$(T/300)^{-0.1}$	D
$OH + HONO \rightarrow H_2O + NO_2$	1.8E−11,390	D
$CH_3O_2 + NO_2 + M \rightarrow CH_3O_2NO_2 + M$	k_o: 1.5E−30$(T/300)^{-4.0}$; k_8: 6.5E−12$(T/300)^{-2.0}$	D
$CH_3O_2NO_2 + M \rightarrow CH_3O_2 + NO_2 + M$	K_{eq}: 1.3E−28,−11200	D
$CH_3C(O)O_2 + NO_2 + M \rightarrow PAN + M$	k_o: 9.7E−29$(T/300)^{-5.6}$; k_8: 9.3E−12$(T/300)^{-1.5}$	D
$PAN + M \rightarrow CH_3C(O)O_2 + NO_2 + M$	K_{eq}: 9.0E−29,−14000	D
$OH + CO \rightarrow H + CO_2$	1.5E−13(1 + 0.6P)	D
$OH + CH_4 \rightarrow CH_3 + H_2O$	7.44E−18T^2,1361	A94
$OH + H_2O_2 \rightarrow H_2O + HO_2$	2.9E−12,160	D
$OH + CH_3OOH \rightarrow H_2O + CH_3O_2$	2.66E−12,−200	D
$OH + CH_3OOH \rightarrow H_2O + CH_2O + OH$	1.14E−12,−200	D
$OH + CH_2O \rightarrow H_2O + HCO$	1.0E−11,0	D
$OH + H_2 \rightarrow H_2O + H$	5.5E−12,2000	D
$OH + SO_2 + M \rightarrow HOSO_2 + M$	k_o: 3.0E−31$(T/300)^{-3.3}$; k_8: 1.5E−12	D
$HOSO_2 + O_2 \rightarrow HO_2 + SO_3$	Fast	
$SO_3 + 2\ H_2O \rightarrow H_2SO_4 + H_2O$	Fast	
$OH + C_2H_6 \rightarrow H_2O + C_2H_5$	1.51E−17T^2,492	A94
$OH + C_2H_4 + M \rightarrow C_2H_4OH + M$	k_o: 1.0E−28$(T/300)^{-0.8}$; k_8: 8.8E−12	D
$OH + C_2H_2 + M \rightarrow C_2H_2OH + M$	k_o: 5.5E−30; k_8: 8.3E−13$(T/300)^{2.0}$	D
$OH + C_3H_8 \rightarrow H_2O + C_3H_7$	1.48E−17T^2,39	A94
$OH + C_3H_6 + M \rightarrow C_3H_6OH + M$	k_o: 8.0E−27$(T/300)^{-3.5}$; k_8: 3.0E−11	D
$OH + i - C_4H_{10} \rightarrow H_2O + C_4H_9$	1.11E−17T^2,−256	A94
$OH + n - C_4H_{10} \rightarrow H_2O + C_4H_9$	1.55E−17T^2,−180	A94
$OH + i - C_5H_{12} \rightarrow H_2O + C_5H_{11}$	2.11E−17T^2,−223	A94
$OH + n - C_5H_{12} \rightarrow H_2O + C_5H_{11}$	2.11E−17T^2,−223	A94
$OH + C_3H_6O \rightarrow H_2O + C_3H_5O$	5.34E−18T^2,230	A94
$OH + C_2H_6S \rightarrow$	1.20E−11,260	D
$OH + C_5H_8 + M \rightarrow C_5H_8OH + M$	k_o: 1.0E−26; k_8: 2.54E−11,−410	D

Rate constants listed as $a.b$E$-cd,efg$, which should be read as $a.b \times 10^{-cd}\exp(-efg/T)$.

Fast = rate is assumed to be very fast in the troposphere.

The alkyl radical fragments produced in OH plus NMHC reactions associate with oxygen rapidly to produce RO_2 radicals.

Reactions for which k_o and k_8 are listed are evaluated by the Troe expression [see *DeMore et al.*, 1997].

Reactions that list equilibrium constants calculated using this K_{eq} value and the rate coefficient for the reverse reaction.

References: A92 = *Atkinson et al.* [1992]; A94 = *Atkinson* [1994]; D = *DeMore et al.* [1997]; E = *Elrod et al.* [2001].

photochemical activity that proceeds northward in concert with the availability of solar radiation and radical precursors including water vapor [*Klonecki and Levy*, 1997; *Yienger et al.*, 1999].

2.2. Steady State Model

[18] A simple numerical model was constructed based on the assumption of steady state for each member of the HO_xRO_x family [*Cantrell et al.*, 1996a]. For each radical (OH, HO_2 and RO_2), if the time derivative of the concentration is small compared to production and loss then this approximation is valid.

$$\frac{d[R]}{dt} = P - L[R] \approx 0 \tag{11}$$

[19] Therefore, $P_R \approx L_R[R]$ and $[R]_{ss} \approx P_R/L_R$, where P_R is the sum of the production rates of radical R, and L_R is the sum of the pseudo-first-order loss rate coefficients of R. This method will lead to accurate estimates of R if the chemical mechanism is complete, rate coefficients are accurate and if d[R]/dt is indeed small. The error in $[R]_{ss}$ due to the latter factor is approximately $d[R]/dt/P_R$. For TOPSE, P_R values were typically 10^5 to 10^6 cm^{-3} s^{-1}. If R changed by 10^8 cm^{-3} over 4 hours (say due to change in j-values over a diurnal cycle), then d[R]/dt would be

7×10^3 cm^{-3} s^{-1}, and the steady state [R] would be in error by 0.7–7% (depending on P_R). Uncertainties in steady state radical levels due to uncertainties in rate coefficients [*DeMore et al.*, 1997; *Sander et al.*, 2000] and measured concentrations of quantities used to constrain the equations (e.g., j-values, NO, O_3, CO, CH_4, etc.) were estimated using a Monte Carlo approach (as in the work of *Cantrell et al.* [1996b]) leading to 2-sigma uncertainty estimates in the calculated radical concentrations of about 41%. This estimate does not include systematic errors that would be caused by an incomplete mechanism, or inappropriate application of the steady state approximation. This approach, except in situations of, for example, rapidly changing solar intensity due to intermittent cloud cover, is expected to lead to a reasonable representation of atmospheric radical levels. The mechanism employed is summarized in Table 1. Measurements of the following species were used to constrain the calculations: pressure, temperature, H_2O vapor, NO, NO_2, O_3, CO, CH_4, H_2O_2, CH_3OOH, CH_2O, PAN, HNO_3, CH_3ONO_2, SO_2, DMS, ethane, ethene, ethyne, propane, propene, i-butane, n-butane, i-pentane, n-pentane, isoprene, jO_3, jCH_2O, jH_2O_2, jCH_3OOH, jacetone, jHONO, $jHNO_3$, jPAN, jCH_3ONO_2 and jNO_2 (for PSS calculations); H_2 was fixed at 550 ppbv; acetone was calculated from CO ([acetone, pptv] = −126.8 + 6.12 [CO, ppbv] [*McKeen et al.*, 1997]) based on measurements of *Singh et al.* [1994]. Carbon monoxide (CO) concentrations ranged from about 60 to 240 ppbv, yielding acetone concentrations ranging from 245 to 1320 pptv, within the range of values reported in the literature. Acetone makes little difference to free radical budgets in the present case, however, because photolysis of acetone is not an important radical source at the altitudes studied, nor is acetone an important OH reactant relative to CO and CH_4.

[20] Two separate calculations were performed. (1) The hydrocarbon reactivity toward OH is approximated by calculating a total equivalent CH_4 concentration corresponding to the sum of that for each measured organic compound ($CH_{4,equiv} = \Sigma[HC]k_i/k_{CH4}$, where k_i values refer to reaction with OH). Thus, three radical concentrations are derived, OH, HO_2 and CH_3O_2. (2) A steady state equation is derived for each peroxy radical corresponding to each measured organic compound. Thus, concentrations are derived for OH, HO_2, and each of the respective RO_2 (including CH_3O_2) radicals. For each of these calculations, peroxynitric acid (HO_2NO_2) and methylperoxy nitrate ($CH_3O_2NO_2$) were also assumed to be in steady state and were calculated along with the free radicals. The assumption of steady state for these peroxynitrate species may or may not be valid, but the inclusion of these processes does not greatly impact the radical levels. Steady state concentrations of reservoir and other species (CH_2O, H_2O_2, CH_3OOH, PAN, and HONO as well as O_3) were calculated separately. The steady state radical concentrations and the measured quantities were used in the P_R and L_R terms for these reservoir species. The lifetimes ($1/L_R$) of the reservoir species can certainly be long enough that the steady state assumption (that $P_R \approx P_L$) is not valid, and could explain some of the measurement-model differences found for these species. However, just because a long lifetime is calculated for a given species, does not necessarily mean that its concentration will differ greatly from steady state. The lifetime gives an indication of the time to arrive at steady state, but if the concentration is already there, a long lifetime does not guarantee that a species is not in steady state.

[21] To solve the system of n equations and n unknowns, the Newton-Raphson iterative method is employed [*Press et al.*, 1992]. An initial estimate of each radical concentration is required and then succeeding calculations are performed until results from successive iterations change the derived radical amounts by a small fractional amount (typically 10^{-4}). Altitude-time profiles of steady state derived HO_xRO_x concentrations that overlap the HO_xRO_x measurements are shown in panels (c) and (d) (Figure 1). The ratios between the HO_xRO_x measurements and the steady state results (ratios calculated first and then smoothed contours determined) are shown in panels (e) and (f) of Figure 1. There are similarities to and differences between the measured and steady state peroxy radical estimates, but in general the agreement is quite good. The average ratios are 1.04 (±0.73) and 0.96 (±0.52) for the MLB and HLB, respectively. Noticeable differences include systematically high measurements in the early part of the campaign (higher in the MLB), which may be due to measurements near the detection limit (which have greater uncertainty), and systematically low values in the middle period (about days 80 to 120), possibly a result of lower data coverage. Except for the very highest values before day 60 in the MLB, the other differences are within the combined uncertainty of the measurements (±35%) and the steady state model (±41%). A comparison of the differences between measured and modeled HO_xRO_x versus temperature shows good agreement at lower temperatures (−60 to 0°C), but the measurements are systematically higher than the model at higher temperatures (0 to 20°C); the latter could be due to complex hydrocarbon chemistry not considered in the model that becomes important near landing at Jeffco, which is close to the Denver metropolitan area.

3. Budgets of Peroxy Radicals

[22] We can examine the production and loss processes for individual species or for families from the model results. The importance of various processes in the formation and destruction of these groups will be examined. The rates of the various production and loss terms come from the steady state model constrained by measurements of relevant species. Notice that the production rates require no modeling to calculate, since they depend entirely on observed quantities. For example, the production rate of HO_2 from CH_2O photolysis is $j_4[CH_2O]$; both of these quantities were measured.

3.1. Sources of HO_xRO_x

[23] Radicals are produced by a variety of photolytic and thermal reactions with relative importance that varies depending on the concentrations of the corresponding precursor species, light levels, temperature and humidity. The important photolytic processes are reaction (3) (representing the radical forming process in the UV photolysis of ozone), reaction (4), and others such as the photolysis of peroxides (e.g., H_2O_2 and CH_3OOH) and carbonyl compounds (e.g., acetaldehyde and acetone). Several studies

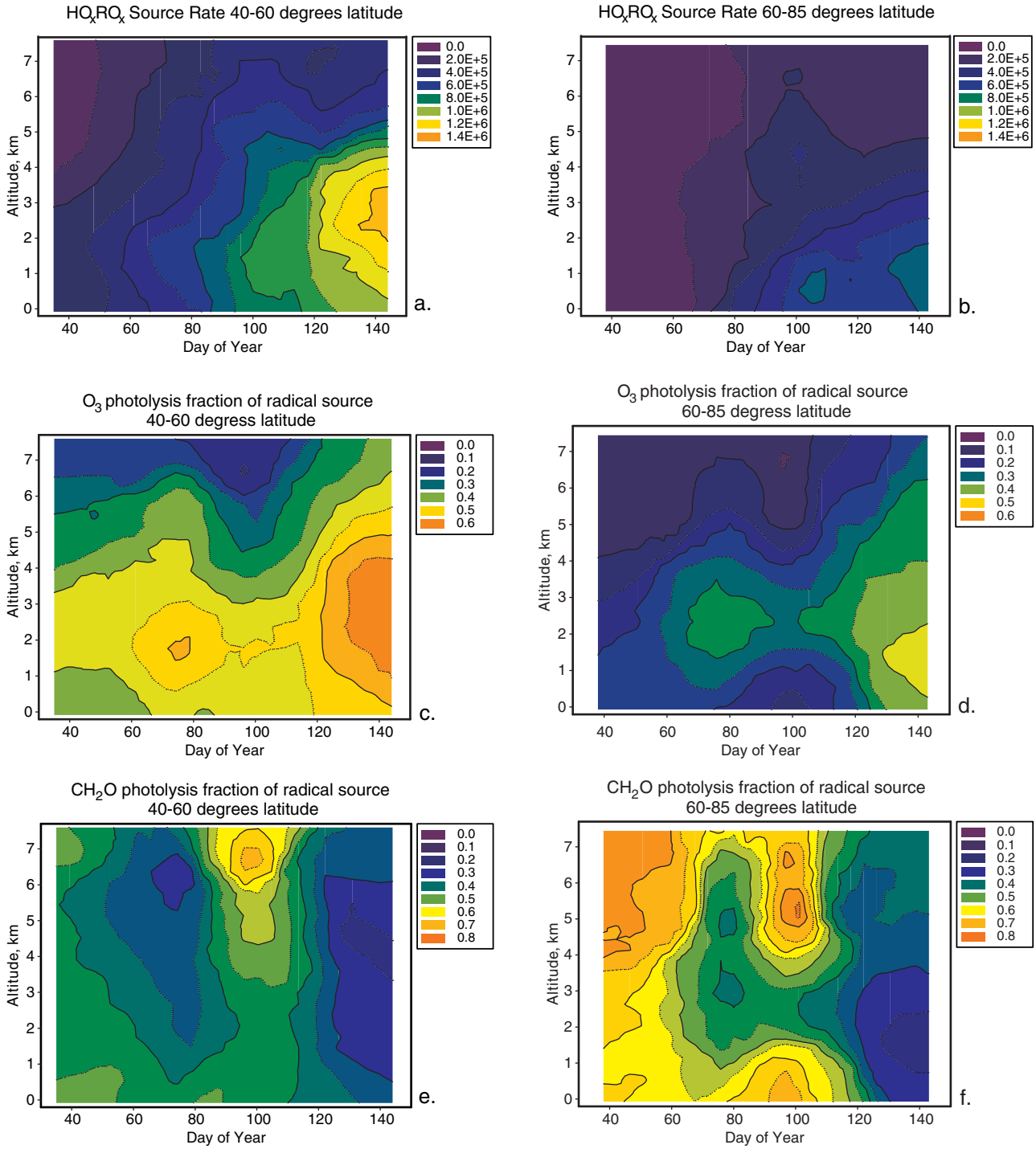

Figure 2. Altitude-time profiles of the total HO_xRO_x source (a, b) calculated from observations, fraction of this source due to reaction of $O(^1D)$ with water vapor (c, d), and fraction due to photolysis of formaldehyde (e, f) for the MLB (left) and HLB (right) regions.

have proposed separating HO_xRO_x sources into primary and secondary [*Wennberg et al.*, 1998; *Jaeglé et al.*, 1998, 2000, 2001; *Crawford et al.*, 1999; *Hauglustaine et al.*, 1999]. The argument is that one should separate radical sources that are independent of the local HO_xRO_x concentration (primary) from those that are locally produced (secondary). Some species such as peroxides and CH_2O fall into both categories (transported by convection from a region of higher productivity, for example, and locally produced). We begin by not separating these processes into primary and secondary, and therefore define HO_xRO_x sources as the sum of rates of all of the source reactions.

[24] Panels (a) and (b) of Figure 2 show altitude-time profiles for the calculated total HO_xRO_x source rate ($P_{HO_xRO_x}$) at the two latitude bands described earlier (MLB and HLB). We see very low rates in the early part of the measurement

period that increase systematically with season. The HLB lags the MLB by 40–50 days at the surface, and more at higher altitudes. This summary plot does include variability due to cloud effects on solar radiation and the effect of the fact that measurements were performed at different times of day, since no filtering or correction for these effects was performed. It is assumed that the diurnal cycle is sampled sufficiently for these values to be representative of midday average values.

[25] How do the individual sources (calculated from measured quantities) contribute to the total HO_xRO_x production rates? Panels (c) and (d) of Figure 2 show altitude-time profiles of the fraction of the total source contributed by $O(^1D)$ plus water vapor. Notice that the contribution from this reaction (often termed the most important source of HO_xRO_x throughout the troposphere) is very small in the early part of the study period at all latitudes, and remains small through most of the study period at high latitudes. What then produces HO_xRO_x here? Panels (e) and (f) of Figure 2 show the contributions from CH_2O photolysis (reaction (4)). H_2O_2 photolysis contributes about 10% in the MLB and 20% in the HLB of the total source, on the average. These two processes (j(CH_2O) and j(H_2O_2)) are significant sources at middle to high altitudes (>4 km) from the beginning of the study until about the end of April. Other less important sources include photolysis of CH_3OOH (about 10% of the total source) and photolysis of acetone (about 2–6% of the total source; acetone is estimated as described above). Here, only the primary production of radicals is considered from these latter two sources; the formaldehyde that is also produced is included in the contribution from CH_2O photolysis. Both of these latter processes contribute slightly more (up to 30% for photolysis of CH_3OOH, and up to 10% for photolysis of acetone) in the upper altitudes of the study region, with slightly larger roles at the higher latitudes (due to lower water vapor concentrations at the colder temperatures). Note that the rates of radical production from the photolysis of formaldehyde and the peroxides were calculated from the corresponding measured concentrations. Use of the steady state modeled concentrations of formaldehyde and the peroxides affects their fractional contributions as well as the levels of $P_{HO_xRO_x}$. This is because the measured peroxides are well below their steady state values, on the average. There are instances when formaldehyde observations are above steady state [see *Fried et al.*, 2003].

3.2. Sinks of HO_xRO_x

[26] Since the radicals are assumed to be in steady state, in the model, $L_{HO_xRO_x}$ equals $P_{HO_xRO_x}$. Reactions among the HO_xRO_x family members and between HO_xRO_x and NO_y species (NO, NO_2 and HNO_3) act as sinks of radicals, although some sinks are temporary since reactive reservoir species are produced. Reactions (5) (HO_2 self reaction) and (6a)–(6c) (reaction between HO_2 and RO_2) account for most of the loss. Figure 3 shows the fractions these reactions contribute to the total loss for the two latitude bands. Reaction between HO_2 and RO_2, not including CH_3O_2 accounts for 10 to 15% of the HO_xRO_x loss at midlatitudes; the contribution is larger in the early part of the study at high latitudes. Reactions between HO_xRO_x and NO_y species (e.g., NO, NO_2, HNO_3) that result in HO_xRO_x loss contribute about 5–10% to the loss. For the conditions of this study, the HO_2 + OH reaction contributes around 4–10% to the HO_x loss. $RO_2 - RO_2$ reactions are an insignificant component of $L_{HO_x}RO_x$ during TOPSE (<0.1%) and indeed for most tropospheric conditions.

[27] The following section shows how $P_{HO_x}RO_x$ and the measured HO_xRO_x concentrations can be used to infer the apportioning of HO_xRO_x between HO_2, CH_3O_2 and other RO_2. $L_{HO_x}RO_x$ (and thus $P_{HO_xRO_x}$) depends on $(HO_xRO_x)^2$ since the majority of the loss is due to reactions between HO_xRO_x species. This assertion is obvious if the majority of the HO_xRO_x were HO_2, but the conclusion is more subtle for HO_xRO_x which is a mixture of HO_2, CH_3O_2, and RO_2. This proportionality is shown in equation (12). The ratio $L_{HO_xRO_x}/[HO_xRO_x]^2$ depends linearly on the rate coefficients for reactions (5) and (6a)–(6c) (representing the reactions of HO_2 with CH_3O_2, (6′) and other RO_2 (6″)) and the relative amounts of HO_2, CH_3O_2 and the other RO_2 (e.g., $[HO_2]/[HO_xRO_x]$, etc.). Slopes and r^2 correlation coefficients of fits of $P_{HO_xRO_x}$ versus either measured or steady state $[HO_xRO_x]^2$ using normal linear regression (assuming all error in y-variable, units 10^{-11} cm^{3}molecule^{-1}s^{-1}) are 0.98 ($r^2 = 0.88$) and 1.04 ($r^2 = 0.93$) (MLB and HLB, respectively) using the steady state HO_xRO_x, and are 0.79 ($r^2 = 0.85$) and 0.90 ($r^2 = 0.82$) (MLB and HLB) using measured HO_xRO_x. The degree to which these slopes (using steady state or measured HO_xRO_x) agree indicates consistency between the calculated source rate and the measured radical concentrations. These slopes can be used to estimate the partitioning of HO_xRO_x independent of the steady state modeling in the following way. The relationship between $L_{HO_xRO_x}/[HO_xRO_x]^2$, the kinetics of the HO_xRO_x loss processes and the partitioning of HO_xRO_x is presented in equation (12).

$$\frac{L_{HO_xRO_x}}{[HO_xRO_x]^2} = \frac{2\alpha}{1-F}(k_5\alpha + k_{6'}\beta + k_{6''}\gamma) \qquad (12)$$

[28] Where the k values are rate coefficients for the corresponding loss reactions ($k_{6'}$ is the rate coefficient for reaction of HO_2 with CH_3O_2, and $k_{6''}$ represents the weighted average rate coefficient for the reaction of all other RO_2 with HO_2); α, β, and γ are the fractions of HO_xRO_x corresponding to HO_2, CH_3O_2 and RO_2 (not CH_3O_2), respectively, whose sum nearly equals unity (OH member not accounted for, but is always a very small fraction of HO_xRO_x), and F is the fraction of HO_xRO_x lost through HO_xRO_x reactions with NO_y species. So, the ratio $L_{HO_xRO_x}/[HO_xRO_x]^2$ should depend on temperature, pressure, water vapor concentration (through the rate coefficient dependencies) and the radical fractions (which depend on relative abundance of trace gases and relative rates of pertinent processes). Equation (12) was solved for α using steady state or measured HO_xRO_x concentrations for each data point; γ was assumed to be 0.06 (the average value from the steady state results), 1-F was fixed at 0.9 for the HLB and 0.85 for the MLB, and β was set to $1 - (\alpha + \gamma)$. Sensitivity tests were performed to estimate the robustness of α-values determined by this method. Varying α by a factor of 1.35 about the mean value, changed the average difference between the left and right hand sides of equation (12) by 13 to 17%. Given the uncertainties in HO_xRO_x and

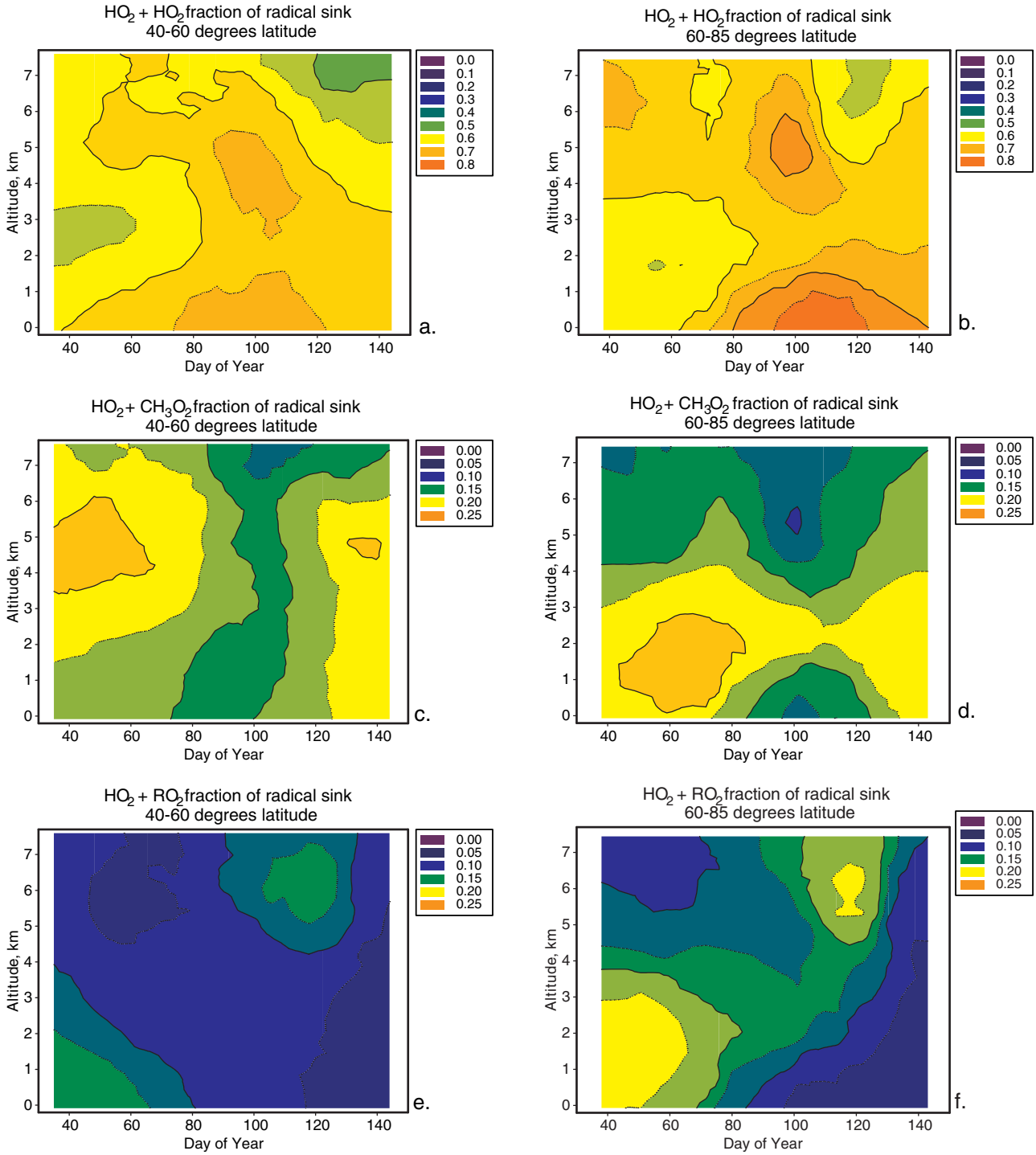

Figure 3. Fractional contributions to $L_{HO_xRO_x}$, as estimated from the observationally constrained steady state model, due to reaction between HO_2 and HO_2 (a, b), HO_2 and CH_3O_2 (c, d) and HO_2 and other RO_2 (not CH_3O_2) for the MLB (left) and HLB (right).

$L_{HO_x}RO_x$ estimates, the α-values derived by this method have uncertainty factors of order 1.5.

[29] Resulting average values of α are shown in Table 2 using both steady state and measured HO_xRO_x. The results are also somewhat sensitive to the choice of k-values in equation (12). Using the recent evaluation of *Tyndall et al.* [2001], $k_{6'}$ is about 10% lower than *Atkinson* [1994] and *Atkinson et al.* [1992] for the TOPSE conditions, and if $k(CH_3CH_2O_2 + HO_2)$ is used for $k_{6''}$, it is about 37% lower; this results in average values for α that are somewhat larger than those determined using Atkinson et al. recommendations. There is scatter in individual α values, due to scatter in the parameters used to derive them. Standard deviations of the means using the steady state HO_xRO_x concentrations are 0.11 to 0.15; for the measured HO_xRO_x they are 0.21 to 0.27. Thus, though the means calculated with steady state

Table 2. HO_xRO_x Radical Distributions Calculated From Total Concentrations and Radical Production Rates (Equation 12)[a]

Method	HO_xRO_x	Rate Coefficients	α MLB	α HLB
Equation (12)	Steady State	*Atkinson* [1994]; *Atkinson et al.* [1992]	0.64	0.69
Equation (12)	Measured	*Atkinson* [1994]; *Atkinson et al.* [1992]	0.53	0.54
Equation (12)	Steady State	*Tyndall et al.* [2001]	0.76	0.78
Equation (12)	Measured	*Tyndall et al.* [2001]	0.61	0.63
Model	Steady State	*Atkinson* [1994]; *Atkinson et al.* [1992]	0.74	0.76

[a] $\alpha = [HO_2]/[HO_xRO_x]$; $\beta = 1 - (\alpha + \gamma) = [CH_3O_2]/[HO_xRO_x]$; $\gamma = 0.06 = [RO_2]/[HO_xRO_x]$.

compared to those using measured HO_xRO_x differ by 0.11 to 0.15, there is overlap within the scatter of these calculations. Given the uncertainties in this method, using the various methods to determine α, the evidence suggests α-values certainly lie between 0.35 and 1.0; for the conditions of TOPSE, they average about 0.5 to 0.8. Thus, the assertion that there are significant errors in $HO_2 + RO_2$ kinetics, and thus very low average tropospheric α values (0.08 to 0.25, corrected for updated water vapor absorption cross-section) as presented by *Stevens et al.* [1997] (for surface measurements in the Rocky Mountains, that may or may not be applicable to conditions of TOPSE) are not supported by the present estimates.

3.3. Budgets of Members of HO_xRO_x

[30] Aspects of the partitioning of HO_xRO_x species can be examined by analysis of the sources and sinks of OH, HO_2, CH_3O_2 and RO_2. The rates of the processes that form these individual family members include HO_xRO_x sources as well as exchange reactions; the loss processes comprise HO_xRO_x sinks along with other exchange reactions. In the following analysis, the fractional contribution of various reactions to the sources and sinks of the HO_xRO_x members are presented, using constrained, steady state model derived quantities.

3.3.1. OH

[31] The sources of OH include the HO_xRO_x source $O(^1D) + H_2O$, reactions of HO_2 with NO and O_3, and photolysis of peroxides. For the MLB, on the average these sources constitute 17%, 42%, 33%, and 8% of the total, respectively. Clearly, an overwhelming majority (75%) of OH comes through HO_2 (reaction with NO and O_3) for these conditions. Although the $HO_2 + NO$ reaction is the largest source on the average, in the lowest 1 km $HO_2 + O_3$ becomes slightly larger. The fractional contribution of $HO_2 + NO$ to the sources shows a regular increase with NO concentration (10% at 1 pptv and 90% at 200 pptv), and also a decreasing role at a given NO concentration as the seasons progress due to the increase in O_3 and temperature (at 10 pptv NO, it is about 55% in the first deployment and about 20% in the last one). The balance of sources are similar at higher latitudes (HLB), but because of the lower temperatures, the corresponding lower water concentration and lower NO concentrations, $O(^1D) + H_2O$ becomes even less important (10%) and $HO_2 + O_3$ becomes more important (43%).

[32] Many reactions act as OH sinks, but the predominant one during TOPSE is OH + CO which, on the average, constitutes 63% of the loss in the MLB. The reaction of OH with CH_4 is next, contributing 12% on the average, but decreasing markedly with altitude due to the large temperature dependence of the reaction rate coefficient. Reactions of OH with O_3, CH_2O, hydrocarbons, SO_2, hydrogen, NO_y species and the peroxides each contribute up to 5%, with an average total contribution to the OH sinks of 25%. The reaction of OH with CO is even a larger fraction of the OH sinks on the average at the higher latitudes (69%).

3.3.2. HO_2

[33] Most HO_2 is formed from reaction of OH with CO, CH_2O, O_3, H_2O_2 and H_2, which contribute in total about 70% throughout the study region on the average (note some of these reactions do not produce HO_2 directly, but the products react rapidly with O_2 to produce HO_2). The reaction of OH with CO is the most important (about 70% of the OH reactions). Photolysis processes (CH_2O, CH_3OOH) contribute 18% and 22% in the MLB and HLB, respectively. The balance is formed from the reaction of RO_2 and CH_3O_2 with NO (12% and 9%, respectively).

[34] There are three nearly comparable processes that destroy HO_2, namely reaction of HO_2 with NO, with O_3, and with HO_2. Due to the changes in temperature and NO in the two latitude bands, their relative importance changes slightly. The $HO_2 + NO$ fractional contribution is larger than $HO_2 + O_3$ in the MLB (39% and 29%, respectively) while their relative roles switch in the HLB (32% and 36%, respectively). The $HO_2 + HO_2$ reaction contributes about 22% in both regions.

3.3.3. $CH_3O_2 + RO_2$

[35] The most important sources of organic peroxy radicals, on the average, are the reactions of OH with methane (50–46%), other hydrocarbons (23–30%), and CH_3OOH (14–11%) for the MLB and HLB, respectively. The estimated contribution from the photolysis of acetone, on the average, is 9% and 12% in the two latitude bands. Thermal decomposition and photolysis of PAN contribute about 2% on the average, although they can contribute up to 10% at low altitudes and middle latitudes where the temperature is higher. The thermal decomposition of methylperoxy nitrate ($CH_3O_2NO_2$) is about 35% (on the average) of the total $CH_3O_2 + RO_2$ production rate, but is exactly balanced by its production rate; thus, the chemistry of this species does not impact the organic peroxy radical concentrations, even though there can be a significant flux through it.

[36] The average contributions to the sources and sinks of these radicals in the two latitude bands are shown on Figure 4.

[37] Cycling of radicals is important in the TOPSE study region and at other locations in the troposphere. We can estimate the efficiency of cycling during TOPSE from the rates of cycling and the rates of termination for HO_xRO_x. The cycling to termination rate ratio may be termed the

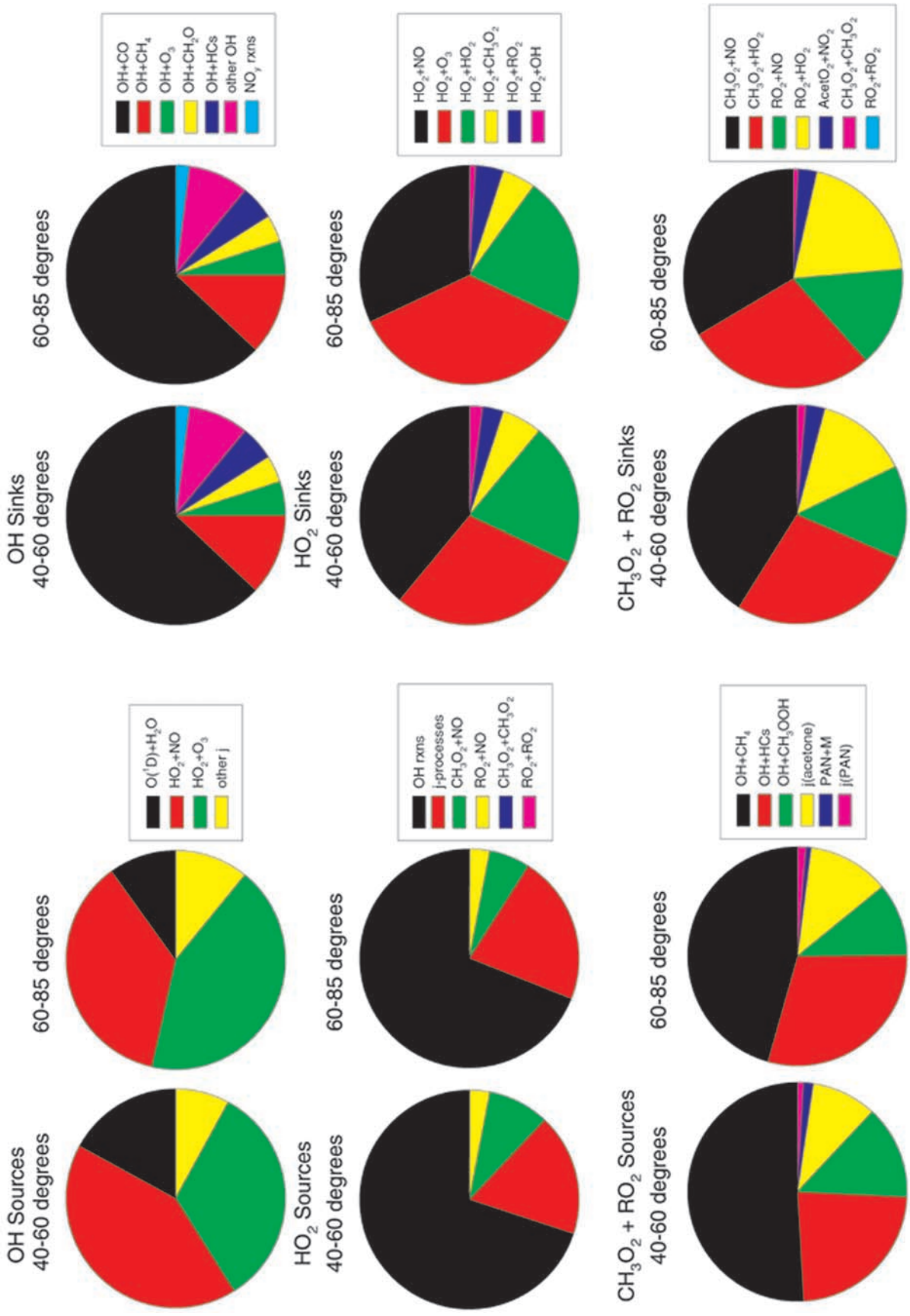

Figure 4. Average fractional contributions of processes to sources (calculated from observations) and sinks (estimated from observationally constrained steady state model) of HO_xRO_x members for the MLB (left graph of a pair) and the HLB (right graph of a pair).

chain length, since it describes the average number of propagation cycles a radical makes before removal. Since the individual radicals (OH, HO_2, etc.) as well as the HO_xRO_x family are assumed to be in steady state, then the conversion rates from any member to any other are equal. Using the conversion rates of HO_2 to OH (estimated from the steady state model) for each data point yields average chain lengths and standard deviations of 2.2 (σ = 2.0) and 2.1 (σ = 1.2) for the MLB and HLB, respectively. There is scatter in these calculated chain lengths due to changes in rates of various processes with zenith angle, season, and trace gas concentrations. The chain lengths are generally smaller at larger $j(O(^1D))$ values due either to seasonal or diurnal changes. Larger NO concentrations, larger $P_{HO_x}RO_x$ rates, and higher altitudes generally lead to larger chain lengths. Averages are 3.3 and 1.6 for the altitude band from 0.2 to 1 km in MLB and HLB, respectively. Corresponding values are 2.2 and 2.3 for altitudes greater than 6 km.

[38] The steady state model results can tell us something about the partitioning of members of the HO_xRO_x family by looking at ratios of various species and the factors controlling these ratios.

3.3.4. HO_2/OH

[39] This steady state model calculated radical ratio ranges between about 80 and 800 with clear dependencies on altitude, latitude and deployment (season). The average ratios are higher at lower altitudes, at higher latitudes, and at earlier deployments. This is the result of temperature differences which affect the kinetics of conversion reactions, and differences in trace gas concentrations that affect the rates of exchange reactions. The altitudinal gradient (lower ratios at higher altitudes) is large in the earlier part of the study, and is much smaller by the end. A component of these trends is also reflected in the change in relative lifetime of these two species. The values approach those expected and calculated for tropical and midlatitudes, about 100, when photochemical activity is high. This ratio can be approximated by the simple formula in equation (13), which reproduces the steady state results quite well (although not perfectly).

$$\frac{[HO_2]}{[OH]} = \frac{k_{CO}[CO] + k_{CH2O}[CH_2O] + k_{O3}[O_3] + k_{H2O2}[H_2O_2] + k_{H2}[H_2]}{k_8[NO] + k_{O3}[O_3]} \quad (13)$$

[40] The rate coefficients in the numerator represent reaction between OH and the corresponding species; in the denominator they represent reactions with HO_2. The ratios from equation (13) average 178 in the MLB, and 246 in the HLB; corresponding steady state ratios average 168 and 240. The ratio can also be estimated from the radical measurements; this is limited because of problems with the OH measurements in the early part of the campaign and at altitudes greater than about 3 km [*Mauldin et al.*, 2003], and the fact there are very few HO_2 measurements. Thus, HO_2 is estimated from the HO_xRO_x measurements by scaling for an estimated HO_2/HO_xRO_x ratio of 0.75 in this case. This derived HO_2 is combined with the OH measurements where they overlap. Steady state HO_2/OH ratios are also retrieved at the same data points. There is considerable variability, and the correlations between measured and steady state ratios are low (r^2 values of 0.14 and 0.08 for the MLB and HLB). Average ratios are similar for these overlapping conditions; HO_2/OH average measurement-derived ratios are 173 and 176 in the MLB and HLB and the average steady state ratios for the same points are 179 and 178. There are 102 and 199 coincident points for MLB and HLB; standard deviations of these averages are about 100. The average steady state HO_2/OH ratio for all points (7529) is 235, but this varies greatly with NO and CO level. The steady state HO_2/OH ratio decreases with increasing NO concentration as noted by other workers, and expected based on equation (13). The calculated ratio averages about 600 at 1 pptv NO, and is about 45 at 100 pptv NO. These calculated ratios also increase with increasing CO, as expected. As an example, at 10 pptv NO, HO_2/OH increases from 96 at 100 ppbv CO to 230 at 160 ppbv. For all NO values, the calculated ratio varies from about 100 to 250 over the same CO range.

[41] Previous studies of the HO_2/OH ratio in the troposphere include *Cantrell et al.* [1996a], *Stevens et al.* [1997], *Brune et al.* [1998, 1999], *Carslaw et al.* [1999a, 1999b], *Creasey et al.* [2001], and *Kanaya et al.* [2001]. There have also been a number of studies in the upper troposphere and lower stratosphere at altitudes greater than about 10 km [e.g., *Cohen et al.*, 1994; *Wennberg et al.*, 1994, 1998; *Lanzendorf et al.*, 2001], where the observed ratios are 5 to 20. In the lower and middle troposphere, previously reported mean ratios range between about 40 and 200, depending on altitude and NO level. Individual observations can be much higher or lower. The average of these reported means is 95 for an average NO of 50 pptv. Reported model ratios tend to be higher, sometimes by large factors [*Stevens et al.*, 1997; *Tan et al.*, 1998].

[42] For TOPSE, average modeled ratios are within a few percent of average measurement-derived ratios for overlapping conditions. The estimated uncertainty in the steady state model calculated HO_2/OH ratios is 43% (2σ); the uncertainty in the measurement-derived ratios is estimated to be 70% (2σ).

3.3.5. $HO_2/(HO_xRO_x)$

[43] For the conditions of TOPSE, model calculations indicate that the peroxy radicals are primarily in the form of HO_2 most of the time. From the steady state model results, this ratio averages 0.74 in the MLB and 0.76 in the HLB. The presence of enhanced hydrocarbon levels in the early part of the campaign [*Blake et al.*, 2003] slightly reduces this ratio as RO_2 radicals are produced at the expense of HO_2. Low hydrocarbon concentrations yield an average ratio of about 0.8 and higher concentrations, a ratio of about 0.65. The ratios are also higher at lower temperatures due to the reduction in the rate coefficient for OH reactions with methane and other hydrocarbons. The average ratios are in good agreement with the concentration-loss rate correlation presented earlier. There was not sufficient HO_2 data collected to allow this ratio to be estimated directly from measurements.

3.3.6. $CH_3O_2/(HO_xRO_x)$

[44] Methyl peroxy radicals are calculated from the steady state model to be the most abundant RO_2 during

TOPSE accounting for 23% of HO_xRO_x on the average in both latitude bands.

3.3.7. RO_2 (Not CH_3O_2)/(HO_xRO_x)

[45] Organic peroxy radicals (other than CH_3O_2) are calculated from the steady state model to contribute a fairly small fraction to HO_xRO_x during TOPSE, averaging 0.06 in both latitude bands. The apportioning among the various types of RO_2 was about the same in the MLB and HLB. On the average, acetylperoxy radicals are calculated to have the largest contribution (18% of RO_2, not CH_3O_2). Next, in order of average concentration were the peroxy radicals derived from propene, propane, isoprene, ethane, ethyne and n-butane with percentages of 17, 12, 12, 9, 8, and 7, respectively. The peroxy radicals derived from acetone, i-butane, i-pentane, n-pentane contribute 2 to 4% on the average.

3.4. Comparison of Equivalent Methane to Explicit Calculations

[46] As described above, two parallel steady state calculations were performed which either accounted for hydrocarbon reactivity as equivalent methane, or followed the reaction of OH with each hydrocarbon. The average ratios of the first to the second calculation for OH, HO_2 and CH_3O_2 are 0.90, 0.88, and 0.92, respectively, with 1 sigma standard deviations of the means of about 0.1. There are a few individual calculations, however, which show significant differences. For most purposes, the equivalent methane approach is sufficiently accurate to understand overall tropospheric peroxy radical behavior in a more straight forward manner than the full steady state calculation. It might also be possible to parameterize the HO_xRO_x loss processes (for example, use a weighted average of the $HO_2 - RO_2$ loss rate coefficients that accounts for the presence of different RO_2 radicals) to improve the performance of the equivalent methane approach, but this has not been done here. In the absence of nonmethane hydrocarbons, the two approaches yield identical results. The equivalent methane approach is an attempt to account for the enhanced production of RO_2 as NMHC concentrations increase, but it is not exact because of the approximate accounting of RO_2-HO_2 loss rates by assuming all RO_2 radicals are CH_3O_2.

3.5. Radical Reservoirs

[47] Many of the products of HO_xRO_x loss reactions are, in fact, temporary radical reservoirs that can act as radical sources. This is noticeable if these reservoir species are formed in an area of high photochemical activity (high radical production rate) and transported to areas of lower activity (e.g., by convective transport from the boundary layer to higher altitudes, or by transport from urban to more remote areas) in that photolysis of these reservoir species can then play a proportionately greater role than would be at photochemical equilibrium. The effectiveness of these transport processes depends on the lifetime of these reservoir species, and perhaps also their solubility in cloud droplets and/or reactivity on aerosol surfaces that would result in loss along the transport trajectory. Important reservoir species include peroxides (H_2O_2, CH_3OOH and ROOH), peroxy nitrates (HO_2NO_2, $CH_3O_2NO_2$ and PAN) and carbonyl compounds (CH_2O and others). Carbonyl compounds can have sources other than tropospheric photochemistry (e.g., biogenic emissions), and are formed from reactions in the atmosphere not initiated by free radicals, such as between ozone and alkenes. The overall role of these species in atmospheric chemistry is a complex one beyond the scope of this paper. We seek here to generally understand their importance to tropospheric free radical chemistry in the context of TOPSE.

[48] The gas-phase lifetimes of the peroxides and formaldehyde are governed by loss due to photolysis and reaction with OH, with rates that depend on solar intensity as modulated by solar zenith angle (SZA) and clouds. At high Sun (25 degrees SZA) for the MLB, average lifetimes are 9.5, 16 and 2.2 hours for H_2O_2, CH_3OOH, and CH_2O, respectively. At low Sun (85 degrees SZA), the lifetimes extend up to 320, 560 and 85 hours. These lifetimes provide constraints on the degree to which heterogeneous processes can affect the concentrations of these species. They also indicate when measurements of these species could be expected to agree with steady state calculations (i.e., when lifetimes are short compared to time since emission or characteristic lifetime toward heterogeneous loss). One might expect measurement-model differences to increase with the gas-phase lifetime if processes unaccounted in the model were operative. There is no strong indication of such a relationship for peroxides or formaldehyde. Formaldehyde does show a systematic difference between the measurements and the steady state model at very low temperatures, which usually occur at high altitudes and high latitudes [*Fried et al.*, 2003]. The measurements are greater than the steady state model at temperatures less than about −45°C. It appears that other formaldehyde sources, or a change in the known kinetic processes, are operative for these conditions.

[49] There are significant differences between the measured and steady state modeled peroxides. Average measurement/model ratios are 0.41 and 0.78 for H_2O_2 and CH_3OOH in the MLB, respectively; corresponding values in the HLB are 0.42 and 0.68. The ratios show no dependence on temperature, zenith angle or lifetime of the respective peroxide, although the ratios are larger at the lowest steady state concentrations (approximately <200 pptv). The measurement-model differences can be roughly explained by the incorporation of a first-order loss of the peroxides that averages 0.1 and 0.02 hr^{-1} for H_2O_2 and CH_3OOH, respectively; there is a slight reduction in the value needed at higher altitudes. A loss process such as this has been employed in previous studies and is described as the probable loss of peroxides by interaction of air masses with clouds or ice particles [*O'Sullivan et al.*, 1999; *Lee et al.*, 2000]. For PEM-Tropics A and B, *Olson et al.* [2001] report that measurements and models agree sometimes, while the model tends to over predict peroxides at low altitudes (<2 km), and the model is less than the observations at high altitudes (>6 km) on the average. The high altitude (>8 km) peroxide observations in SONEX [*Jaeglé et al.*, 2001] were significantly above model estimates. Detailed modeling studies attempting to understand the impact of the interaction of peroxides (and other trace gases) with clouds have been reported [e.g., *Lelieveld and Crutzen*, 1991; *Kim et al.*, 2002]; recent studies indicate that the perturbation and recovery of peroxide concentrations due to encounter with clouds is complex depending, among other parameters, on the time of day and NO_x levels present. Several studies

[e.g., *Cohan et al.*, 1999; *Mari et al.*, 2000] have described how deep convective clouds could enhance the concentrations of peroxides and formaldehyde in the outflow, consistent with some high altitude observations. While loss rates such as those calculated here are consistent with known rates of cloud encounters, one would expect a high degree of variability in rate required, and indeed sometimes there should be agreement between the measurements and model (e.g., if several lifetimes has passed since the last cloud encounter). It has also been suggested that reaction of HO_2 on aqueous particles produces H_2O_2 [*Jacob*, 2000], which if included in present calculations would make the measurement-model differences even greater.

[50] The effect of using steady state versus measured peroxide and formaldehyde concentrations on the calculated HO_xRO_x levels was also examined. Using steady state formaldehyde decreases the modeled HO_xRO_x at low temperatures to levels below the observations, supporting the enhanced formaldehyde levels observed; using steady state peroxides increases the model radical levels, particularly at temperatures greater than about -20°C, making the measurement-model agreement poorer. These observations indicate that measured peroxides and formaldehyde are more consistent with the peroxy radical observations than calculated peroxides and formaldehyde.

[51] For temperatures greater than about -20 to -30°C, HO_2NO_2 and $CH_3O_2NO_2$ have lifetimes short enough (less than 1 hour, and approaching seconds to minutes at the highest temperatures) that their concentrations do not build up appreciably (calculated average concentrations of a few pptv or less). At lower temperatures (<-30°C), lifetimes can reach 10 hours and thus the calculated concentrations can be significant. At -50°C, calculated HO_2NO_2 concentrations average 220 and 74 pptv (MLB and HLB, respectively) and $CH_3O_2NO_2$ concentrations average 70 and 27 pptv. These are large enough to impact the NO_y budget (F. Flocke et al., The behavior of PAN and PPN and the budget of odd nitrogen during TOPSE, manuscript in preparation for *Journal of Geophysical Research*, 2003). At temperatures near -50°C, the calculated sum of the concentrations of HO_2NO_2 and $CH_3O_2NO_2$ are 20 to 80% of measured NO_y. More detailed laboratory studies are required to assess the accuracy of kinetic data for the formation and destruction of these species used to calculate their concentrations. Current recommendations [*DeMore et al.*, 1997; *Sander et al.*, 2000] indicate very large uncertainties in these parameters (factors of 2 and 5 in the unimolecular decomposition rate coefficients). In addition, spectroscopic studies to carefully quantify photolytic processes in the ultraviolet, visible and near-infrared spectral regions are also needed to verify those that have been performed [*Zhang et al.*, 2000]; more recent studies do indicate that near infrared photolysis of HO_2NO_2 is indeed important [*Roehl et al.*, 2002]. These uncertainties lead directly to uncertainties in calculated concentrations of these species. For the present calculations, the j-value for photolysis of HO_2NO_2 was assumed to be one-half that of H_2O_2 plus a constant value of 1.5×10^{-5} s^{-1} during daylight hours (slightly larger than the recent *Roehl et al.* [2002] results indicate); the latter is to account for overtone absorption in the red and near-infrared regions. Also, the ultraviolet absorption of $CH_3O_2NO_2$ is similar to HO_2NO_2 and even though there is no specific evidence for the overtone absorption, the total j-value for $CH_3O_2NO_2$ was assumed to be the same as that for HO_2NO_2 in most calculations.

[52] The PAN lifetime is about an hour at 20°C. PAN lifetimes depend on a number of factors including temperature, zenith angle, and the NO_2/NO ratio. The lifetimes range from a few hours at high Sun and warmer temperatures, to more than 10^5 hours (>11 years) at low Sun and the coldest temperatures. At lower temperatures, the lifetime is long enough that the steady state assumption applied here to calculate its concentrations is no longer valid. The ratio of the steady state concentration of PAN to the measured concentration varies systematically with temperature. At -50°C, the average ratios are 2.0 and 1.9 (MLB and HLB, respectively), and at -20°C, they are 0.8 and 1.3. Steady state PAN concentrations are slightly lower than the measurements for PAN lifetimes up to 500–1000 h, and are higher than the measurements for longer lifetimes.

[53] The concentration of other nitrogen species, such as nitrous acid (HONO), can be calculated using the steady state assumption, but here these calculations have not taken into account possible heterogeneous or multiphase processes (e.g., surface emission or deposition, transformation on or within aerosols). The calculated concentrations are quite small, averaging 0.2 and 0.02 pptv in the MLB and HLB, respectively. These concentrations are too small to significantly impact the HO_xRO_x budget. However, if there are other sources operative that could maintain higher steady state concentrations (e.g., in the Arctic boundary layer), photolysis of HONO could be an important source of HO_xRO_x.

[54] It is clearly important to resolve the reasons for these differences between measured and modeled radical reservoir concentrations in order to gain quantitative understanding of tropospheric HO_xRO_x behavior.

4. Ozone Photochemistry

[55] Several studies have examined the various photochemical and transport processes which govern tropospheric ozone [e.g., *Liu et al.*, 1992; *Anderson et al.*, 1994; *Roelofs and Lelieveld*, 1995; *Mauzerall et al.*, 1996; *Klonecki and Levy*, 1997; *Yienger et al.*, 1999; *Kleinman*, 2000]. These studies concur that enhancement of tropospheric ozone results from in situ production and transport of ozone and precursors from source regions (populated midlatitude regions and area of biomass burning). *Yienger et al.* [1999] explain the springtime increase in ozone as a by-product of the atmospheric processes removing NO_x that is built up over winter months. *Klonecki and Levy* [1997] propose that current ozone levels are controlled about equally by photochemistry and transport, in contrast with preindustrial times in which transport was dominant. Mauzerall et al. conclude that in summer at remote northern high latitudes from 0 to 6 km, in situ production constitutes about 2/3 of the gross production which is slightly exceeded by gross photochemical loss, that influx from the upper troposphere constitutes about 1/3 of the gross production which is balanced by surface deposition, and that influx of ozone from mid latitudes amounts to about 10% of the gross production. Following is a comparison of these conclusions with information gathered during TOPSE. In this discussion, measurements of trace gases are used to calculate rates

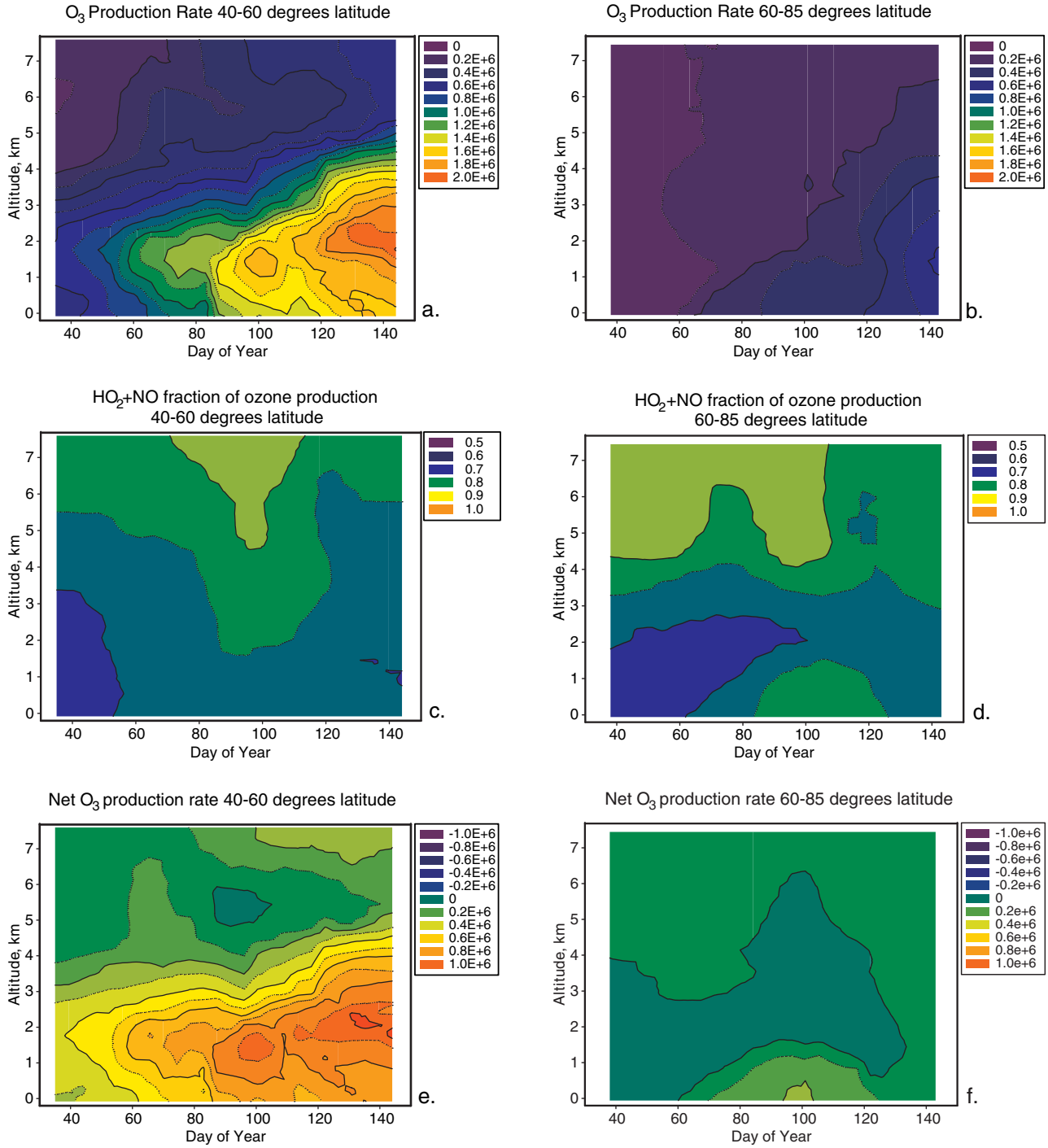

Figure 5. Gross ozone production versus altitude and day of year as estimated from steady state model results for the (a) MLB and the (b) HLB. Fractional contributions to P_{O3} of the reaction of HO_2 with NO versus altitude and day of year for the (c) MLB and the (d) HLB. Net ozone production versus altitude and day of year for the (e) MLB and the (f) HLB.

of reactions except for peroxy radicals. Their concentrations come from the constrained steady model results.

4.1. Sources and Sinks of Ozone

[56] The peroxy radicals are crucial players in the formation and destruction of ozone in the troposphere via gas-phase chemistry. Oxidation of NO by peroxy radicals (reactions (8) and (9a)) comprises the main photochemical source of ozone. This is because of the rapid steady state relationship set up between NO, NO_2 and O_3 [*Cadle and Johnston*, 1952; *Leighton*, 1961].

$$NO_2 + h\nu \rightarrow NO + O(^3P) \quad (14)$$

$$NO + O_3 \rightarrow NO_2 + O_2 \quad (15)$$

$$O(^3P) + O_2(M) \rightarrow O_3 \quad (16)$$

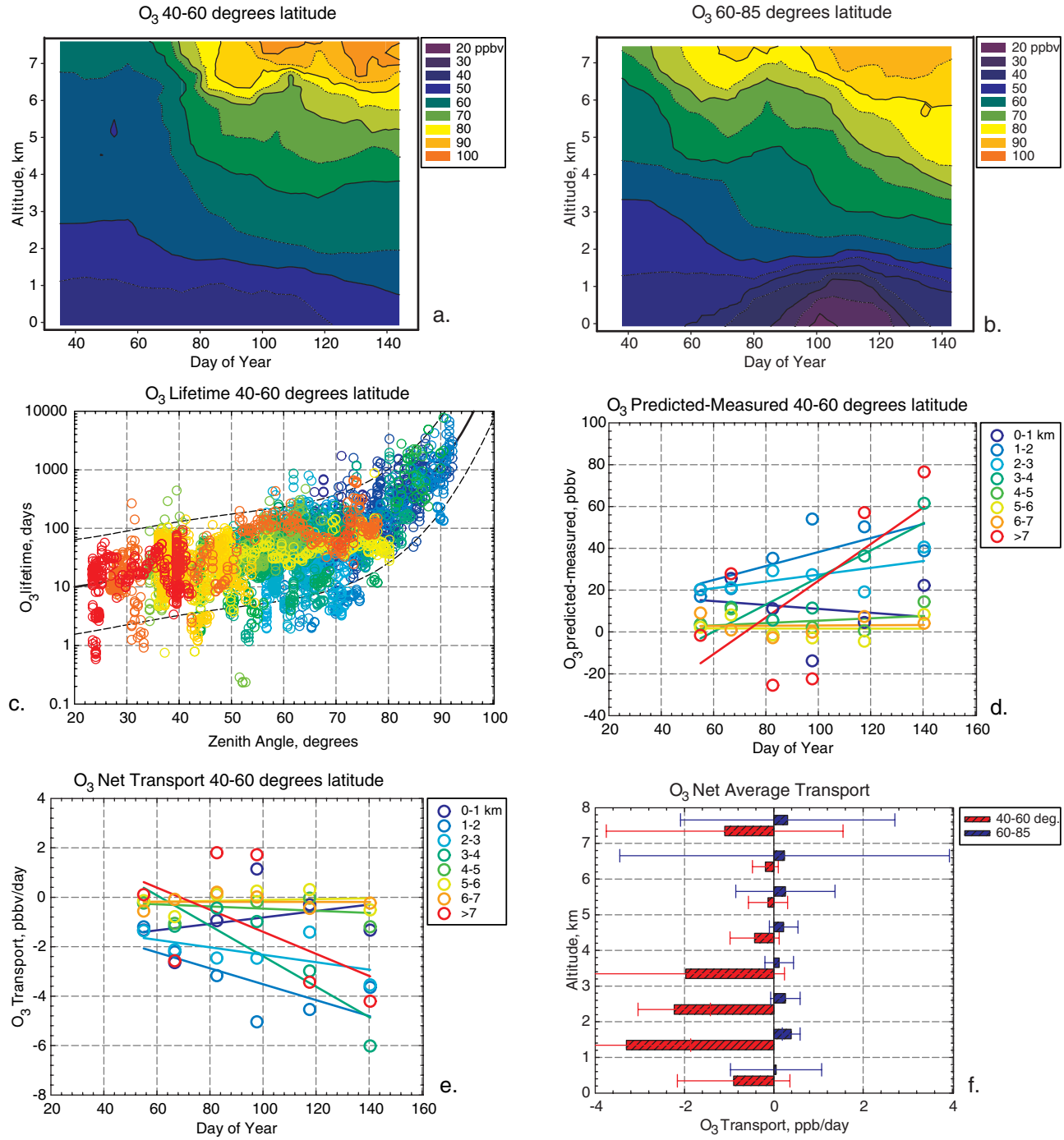

Figure 6. Trends in observed ozone versus altitude and day of year for the MLB (a) and the HLB (b); calculated instantaneous lifetimes of ozone versus zenith angle colored by day of year (violet is at the beginning of TOPSE, red is at the end) for the MLB (c); differences between ozone predicted by equation (18) and measured that have been averaged by deployment into 1 km altitude bins for the MLB (d); calculated net transport of ozone for the MLB (e); net transport of ozone versus altitude for the two latitude bands (f).

[57] This chemistry (reactions (14) through (16)) does not produce ozone, but when NO is oxidized by peroxy radicals (and by any other oxidants except ozone), then ozone is formed because the NO_2 product is later photolyzed, followed by combination of the ground state oxygen atoms with molecular oxygen (reactions (14) and (16)). The rate of reaction of peroxy radicals (from steady state model results) with NO (measured, see *Ridley et al.* [2003]) increased systematically during TOPSE (Figure 5, panels (a) and (b)), with the HLB lagging the MLB by about 100 days in the middle troposphere. The most important source of ozone is the reaction of HO_2 with NO (Figure 5, panels (c) and (d)), accounting for 76% on the average in both latitude bands. Ozone is destroyed photochemically as well. The important

processes include reaction of ozone with OH and HO_2, and photolysis of ozone in the UV-B region (Hartley and Huggins bands) followed by reaction of the $O(^1D)$ product with water vapor; quenching of $O(^1D)$ by N_2 and O_2 (reaction (2)) does not destroy O_3. Photolysis of ozone in the visible spectral region (Chappius band) also does not destroy ozone since only ground state oxygen atoms are produced. The reaction of HO_2 with O_3 (rate calculated using steady state HO_2 and measured O_3) is the most important sink of ozone, accounting for 67% and 80% on the average in the MLB and HLB; its importance decreases slightly as the campaign progressed due to the increasing importance of ozone photolysis. Contributions averaged 78% and 93% at the beginning of the campaign, and at the end they averaged 56% and 70% for the MLB and HLB, respectively.

[58] The net photochemical production of ozone ($P_{O3} - L_{O3}$) during TOPSE is summarized in panels (e) and (f) of Figure 5. Plotted is the difference between the production and destruction rates (calculated using measured species when available and radical species from the steady state model) versus day of year and altitude at the two latitude bands. At midlatitudes, photochemical ozone production exceeds destruction throughout the domain, on the average, and increases through the measurement period. At high latitudes, production and destruction are closely in balance, but there is a slight increase in the net tendency. This can be compared with the observed ozone (Figure 6, panels (a) and (b)). Can net photochemical production explain the observed ozone trend? The midtroposphere (2–5 km) daily averaged ozone trend is 0.08 ppb/day for the MLB, and 0.17 ppb/day for the HLB, through the TOPSE study time period. Net ozone production is positive and increasing throughout the time period in the midlatitude region. The full budget of ozone must also include transport from the stratosphere, advection from other tropospheric regions, and deposition at the surface. An additional term, though minor in a regional sense, in the Arctic region is ozone depletion in the surface layer due to halogen chemistry [*Ridley et al.*, 2003]. The importance of these various processes to the volume averaged ozone abundance depends in part on the photochemical lifetime of ozone. These instantaneous calculated lifetimes are presented in Figure 6 (panel (c)) for the MLB. It can be seen that in the early part of the mission and at large solar zenith angles, the instantaneous lifetime of ozone can be quite long. Later in the mission, at smaller solar zenith angles, and in the surface layer during ozone depletion events, the lifetimes are much shorter. The lifetimes are nearly always long enough so that transport can be a significant component of the regional ozone budget. Estimates of ozone transport from the stratosphere can be made using tracers [*Dibb et al.*, 2003] and 3-dimensional models [*Emmons et al.*, 2003] [*Allen et al.*, 2003]. There is clearly a component of the ozone measured during TOPSE that is of stratospheric origin, but it does not appear that it can explain the trend observed [*Browell et al.*, 2003]. It is likely that a significant fraction of the ozone observed at the beginning of the campaign originated in the stratosphere, but the increase with day of the year is attributed to photochemical formation in the troposphere in the measurement region and along the transport trajectories. Springtime photochemical activity increases significantly over the populated continental regions of the northern hemisphere, resulting in photochemically produced ozone which could be transported northward. Estimating the importance of this process is possible with 3-D models.

[59] The budget of ozone can be described by terms corresponding to chemistry (P_{O3}, L_{O3}) and transport (T).

$$\frac{d[O_3]}{dt} = P_{O_3} - L_{O_3}[O_3] + T \tag{17}$$

[60] Where T represents the net transport related ozone processes including advection, stratosphere-troposphere exchange, and deposition; P_{O3} and L_{O3} represent the chemical processes of production and loss, respectively. Solution of equation (18) leads to the following expression relating the ozone at time, t, to the rates of the chemistry and transport processes (similar to that of *Klonecki and Levy* [1997]), and the ozone concentration at some previous time ($[O_3]_o$).

$$[O_3]_t = \left(\frac{P_{O_3} + T}{L_{O_3}}\right) + \left([O_3]_o - \frac{P_{O_3} + T}{L_{O_3}}\right) e^{-L_{O_3} t} \tag{18}$$

[61] Note that $(P_{O3} + T)/L_{O3}$ equals $[O_3]_{ss}$, the steady state ozone concentration, leading to equation (19).

$$[O_3]_t = [O_3]_{ss} + ([O_3]_o - [O_3]_{ss}) e^{-L_{O_3} t} \tag{19}$$

[62] P_{O3} and L_{O3} average values were calculated from steady state radical concentrations and measured quantities for each of the seven TOPSE deployments and at 1 km altitude bins (P_{O3} and L_{O3} values were calculated for each point along the aircraft flight track and averaged into the bins described). The O_3 concentrations for deployments 2 through 7 are calculated from equation (18) by projecting forward the O_3 concentration based on the photochemical forcing (i.e., P_{O3} and L_{O3}), the average concentration in the previous deployment, and the time between deployments (assuming T is small compared to P_{O3} in this first calculation). For example, the bin average concentration for deployment 2 is calculated using the observed ozone concentration in deployment 1, and the average P_{O3} and L_{O3} for the two deployments. This analysis implicitly assumes that the average P_{O3} and L_{O3} represent a diurnal average (they are averages based on data collected throughout the daytime), and that these rates are representative (not necessarily constant) of the period between deployments. These assumptions do add uncertainty to these conclusions; the calculated O_3 changes ($[O_3]_t - [O_3]_o$) carry estimated uncertainties of a factor of two. The differences between the predicted (equation (18)) and measured O_3 concentrations are compared in Figure 6 (panel (d)) for the MLB. It is assumed that positive differences (calculated ozone change greater than observed) indicate a net production force is still in effect ($P_{O3} > L_{O3}[O_3]_t$), and that ozone could be exported (thus a negative net transport term). Negative differences (calculated ozone change is less than observed) are assumed to indicate net destruction which must be balanced by import of ozone (positive T). Agreement between predicted and measured ozone is assumed to indicate that the photochemical param-

eters do a good job of explaining the observed trends. Note that the initial ozone chemical tendency ($P_{O3} - L_{O3}[O_3]_o$) does not appear in equations (18) and (19), but that the rate of approach to the steady state value depends on how far the initial concentration is from steady state ($([O_3]_o - [O_3]_{ss})$ and the pseudo-first-order loss rate (L_{O3}) which appears in the exponential term. Of course, in the absence of significant contribution by transport, the rate of change of the ozone concentration is the ozone chemical tendency, but even with no change in values of P_{O3} and L_{O3}, the rate decreases as the concentration approaches the steady state value. The calculated average transport (or other photochemical process) required to balance the ozone budget in each of the altitude, deployment and latitude bins are shown in Figure 6, panels (e), along with grand averages for the entire TOPSE campaign at each altitude for the two latitude bands (panel (f)). These show strong export of ozone from the MLB at 1–4 km of 2–3 ppb/day. There is need, on the average, for a small import of ozone to HLB of 0.1–0.4 ppb/day, much of which likely comes from the MLB, a region of net production, but transport from the stratosphere or upper troposphere (at altitudes above the observations) cannot be excluded. Due to a number of assumptions made in deriving these transport rates, their absolute values are very uncertain, estimated to be greater than a factor of two. These calculated transport rates compare to average P_{O3} values of 6–8 ppb/day (MLB) and 0.7–0.9 ppb/day (HLB). A detailed trajectory analysis or a chemical transport model is required to fully evaluate the role of transport in the ozone budgets of the TOPSE study region, but it does appear that lifetimes are long enough that meridional movement of air with positive ozone productivity or excess ozone could explain the observations.

5. Photostationary State

[63] The recognition of the coupling between the NO_x and HO_xRO_x families has been exploited in a number of observational and theoretical studies [e.g., *Kelly et al.*, 1980; *Calvert and Stockwell*, 1983; *Parrish et al.*, 1986; *Ridley et al.*, 1992; *Hauglustaine et al.*, 1996; *Cantrell et al.*, 1997b; *Carpenter et al.*, 1998]. In this approach, the rapid reactions ((14) through (16)) are presumed to set up a ratio between NO and NO_2 (NO is in steady state) which is governed by the photolysis of NO_2 (jNO_2, the rate coefficient for reaction (14)) and the reaction between NO and O_3 (reaction (15)).

$$\frac{[NO]}{[NO_2]} = \frac{jNO_2}{k_{15}[O_3]} \tag{20}$$

[64] From equation (20) a photostationary state ratio, Φ, is defined.

$$\Phi = \frac{jNO_2[NO_2]}{k_{15}[NO][O_3]} \tag{21}$$

[65] If ozone is the only oxidant of NO to NO_2, then during daylight hours, Φ should be unity. If other oxidants are operative (e.g., peroxy radicals), Φ will increase proportionally, as the $[NO_2]/[NO]$ ratio increases. This leads to an estimate of the peroxy radical level based on deviations of Φ from unity.

$$[HO_xRO_x]_{PSS} = (\Phi - 1)[O_3]\frac{k_{15}}{k_{8,9a}} \tag{22}$$

[66] Here $k_{8,9a}$ represents the weighted average rate coefficient for oxidation of NO by peroxy radicals (HO_2 and RO_2). Equations (21) and (22) can be combined to yield the peroxy radical concentration as a function of measured NO, NO_2, O_3 and jNO_2.

$$[HO_xRO_x]_{PSS} = \frac{k_{15}}{k_{8,9a}}\left(\frac{jNO_2[NO_2]}{k_{15}[NO]} - [O_3]\right) \tag{23}$$

[67] Alternatively, measured HO_xRO_x, O_3 and jNO_2 can be used to estimate the ratio of [NO] to $[NO_2]$.

$$\left(\frac{[NO]}{[NO_2]}\right)_{PSS} = \frac{jNO_2}{k_{8,9a}[HO_xRO_x] + k_{15}[O_3]} \tag{24}$$

[68] *Cantrell et al.* [1997b] estimated uncertainties propagated into $[HO_xRO_x]_{PSS}$ and $([NO]/[NO_2])_{PSS}$ due to uncertainties in the corresponding input parameters, and concluded that $[HO_xRO_x]_{PSS}$ typically has large uncertainties (of order ±60%) while $([NO]/[NO_2])_{PSS}$ uncertainties are of order ±20%. $[HO_xRO_x]_{PSS}$ and $([NO]/[NO_2])_{PSS}$ were calculated from the TOPSE data and the results can be summarized as follows. On the average, the PSS $[HO_xRO_x]$ values were higher than the measurements or the steady state values for NO concentrations less than 20 pptv, while they were in good agreement for NO concentrations greater than 20 pptv. The ratios of PSS to steady state and measured $[HO_xRO_x]$ were calculated from averages binned by NO concentration. The average PSS to steady state HO_xRO_x ratio for NO concentration bins from 20 to 125 pptv is 0.79 (σ = 0.28) using *DeMore et al.* [1997] rate coefficients for reaction (15) and weighted average values for reactions (8) and (9a); the average PSS to measured HO_xRO_x ratio is 0.89 (σ = 0.38). Using revised rate coefficients by *Sander et al.* [2000], the PSS to steady state ratio becomes 0.99 (σ = 0.36), and the PSS to measured is 1.12 (σ = 0.50). For NO concentrations less than 20 pptv, PSS estimated HO_xRO_x is systematically higher than those derived from steady state or the measurements (PSS to steady state ratio is 6.1 (σ = 6.3), and PSS to measured ratio is 6.9 (σ = 7.3) using revised rate coefficients). Since the steady state and measured HO_xRO_x are in good agreement on the average for these low NO conditions, the differences point to errors in PSS-derived values.

[69] One explanation for these PSS-steady state and PSS-measurement differences could be that measured $[NO]/[NO_2]$ ratios are systematically low at the low NO concentrations. This can be checked by comparing PSS-derived (from equation (24) and measured $[NO]/[NO_2]$. The average ratio of $([NO]/[NO_2])_{PSS}$ to $([NO]/[NO_2])_{measured}$ is near unity (1.05, σ = 0.24) at all [NO] concentrations less than 250 pptv (for bins which have a significant number of points), when NO_2 is determined by chemiluminescence (CL) [*Ridley et al.*, 2003]. When NO_2 is measured by laser induced fluorescence (LIF) [*Thornton et al.*, 2000], there are

systematic differences that increase below an NO concentration of about 40 pptv. The average PSS to measured ratio using LIF for NO concentrations between 40 and 250 pptv is 1.35 ($\sigma = 0.46$). For TOPSE, the LIF NO_2 measurements possibly are biased by a small amount and thus appear to be subject greater uncertainty than the CL results.

[70] The cause of overestimated HO_xRO_x by PSS at low NO concentrations appears not to be the NO and NO_2 measurements (when CL results are used), nor to be completely related to rate coefficient uncertainties. Thus the photolysis rate coefficient for NO_2, the O_3 concentration, and possible unknown chemistry remain as explanations. The ratio of PSS to steady state HO_xRO_x is lowered by reductions in jNO_2 or increases in O_3. If measured jNO_2 values are scaled by a factor of 0.9, which brings the PSS to steady ratio nearly in line for NO concentrations less than 20 pptv, the PSS to steady state HO_xRO_x ratio is reduced to 0.06 for NO concentrations greater than 20 pptv; if measured O_3 values are scaled by 1.1 (to approximately bring the PSS to steady state ratios to near unity for NO concentrations less than 20 pptv), the ratio is reduced to 0.14 for the higher NO concentrations. The improvement seen by these scalings in the lowest NO concentration bins is offset by overcorrection in the higher NO concentration bins. The cause of the differences between PSS estimates of HO_xRO_x and the measurements and steady state calculations at lower NO concentrations remains unknown at this time.

[71] The presence of additional oxidants of NO in the atmosphere is possible and has been postulated to explain the difference between PSS and observations. For example, halogen oxides (ClO, BrO and IO) react with NO to produce NO_2. The average calculated concentrations of halogen oxides are low, averaging 0 ($\sigma = 4-5$) pptv, although it is known that halogen chemistry can be very important in the Arctic boundary layer [*Ridley et al.*, 2003]. *McElroy et al.* [1999] have suggested that BrO levels of 10 pptv throughout the free troposphere (1 to 5 km) are consistent with spectral measurements in the Arctic. The TOPSE measurements on the average, do not support this contention. Within the uncertainties of the observations and kinetic parameters that are involved in controlling NO/NO_2, the data do not completely rule out the presence of a small concentration (2–5 pptv) of halogen oxides throughout the troposphere.

[72] Comparison of the PSS derived quantities (e.g., HO_xRO_x and NO/NO_2) and measurements provides important tests of some aspects of tropospheric photochemistry, and should continue to be applied to tropospheric observational studies, while recognizing the uncertainties necessarily associated with the PSS approach.

6. Summary

[73] Peroxy radicals and many other species were measured over the winter-to-spring transition from middle to high latitudes in the year 2000 during the TOPSE campaign. This is the most complete observational data set collected to date over this geographical and temporal domain, and can serve as a powerful test of our understanding of tropospheric free radical chemistry. A steady state model that was constrained by the measured species generally reproduces the measured concentrations of HO_xRO_x well. Radical budgets reveal differences compared to "conventional" ideas about radical sources, most notably that the reaction of $O(^1D)$ with water vapor is not as important as in the low and midlatitude lower troposphere. The photolysis of formaldehyde is a very important source of HO_xRO_x for this study. Members of the HO_xRO_x family are formed through a variety of radical conversion processes that set up fairly robust concentration ratios. In some cases, the ratios can be explained by only a few reactions.

[74] Examination of radical reservoir species reveals some inconsistencies between measurements and steady state model results, particularly in the case of the peroxides. In the past, significant disagreements between measured and modeled formaldehyde were noted, but on the average there is satisfactory agreement in this study with some exceptions observed at very low temperatures ($<-45°C$). The measured peroxide concentrations are consistently and significantly less than those inferred from the steady state model as found in some previous studies for certain altitudes. Heterogeneous processes have been postulated in the literature to explain these differences, but lifetime considerations presented here indicate that there could be problems in our understanding of gas-phase processes. This is certainly an important area to gain quantitative understanding, as hydrogen peroxide is an important oxidant for SO_2 in the aqueous phase, as well as an important indicator of our understanding of tropospheric HO_x chemistry. The roles of peroxynitrate species (HO_2NO_2 and $CH_3O_2NO_2$) were examined. Their abundance is calculated to be significant when temperatures are cold ($<-30°$), and can impact the HO_xRO_x and NO_y budgets. For the TOPSE conditions, though, PAN dominates the NO_y budget and the abundance of thermally labile peroxy nitrates. More laboratory work particularly on the photochemical parameters of $CH_3O_2NO_2$ is needed.

[75] The connection between the peroxy radicals and the photochemical budget of ozone was examined. The net rate of photochemical ozone formation increased through the study period, and is consistent with the observed rate of ozone increase. A simple equation was used to project forward the ozone concentration between deployments. Differences indicate the relative importance of photochemistry and transport on the ozone amounts. The seasonal trends in ozone can be explained by a combination of photochemical production in middle latitudes and transport to high latitudes.

[76] The photostationary state deviations were compared to measurements of HO_xRO_x and the $[NO]/[NO_2]$ ratio. These comparisons indicate that PSS estimates of HO_xRO_x are consistent with measurements at NO concentrations greater than about 20 pptv, but PSS calculated values are systematically higher at lower NO concentrations. The reasons for these differences are not known. PSS estimates of $[NO]/[NO_2]$ are in good agreement with CL NO_x measurements. The concentrations of halogen oxides are constrained to low values (less than a few pptv) by this agreement. PSS remains a powerful test of our understanding of the coupling of NO_x, HO_x and O_x families in the troposphere, although its utility in calculating HO_xRO_x concentrations is limited due to the associated uncertainties.

[77] **Acknowledgments.** The National Center for Atmospheric Research is funded by the National Science Foundation. The authors wish to thank the staff of the Research Aviation Facility of NCAR for their

support of the TOPSE experiment, including operation of the NCAR/NSF C-130 in most difficult conditions. In particular, we thank RAF manager, Jeff Stith; Project Managers: Richard Friesen, Krista Laursen, Allen Schanot; Data Manager: Ronald Ruth; Software Engineers: Janet Anstett, Chris Webster; Chief Pilot: Henry Boynton; Pilots: Lowell Genzlinger, Mike Heiting; Flight Engineer/Chief of Maintenance: Edward Ringleman; Flight Engineer: John Cusack; Aeronautical Engineer: Mark Lord; Electrical Engineer: Mike Spowart; Technicians: Kurt Zrubek, John Cowan, Larry Murphy, George Nicoll, Hung Ta, and Bill Irwin; Mechanics: Robert Olson, Ray Crnkovich, Jame Nolan, Brent Kidd, Kip Eagan, and Robert Beasley. Thanks to Ron Cohen's group at the University of California, Berkeley, for the use of their LIF NO_2 observations in this analysis. TOPSE data and other information is available via the Internet at topse.acd.ucar.edu. The arranging of travel for the campaign by Marilena Stone is appreciated. Thanks to helpful, detailed and insightful comments by two anonymous reviewers. The funding of the deployment of the aircraft by NSF through the OFAP and FAC entities, as well as funding of TOPSE participants outside of NCAR by the Atmospheric Sciences Division and Office of Polar Programs of NSF is gratefully acknowledged.

References

Allen, D., J. E. Dibb, K. Pickering, and B. Ridley, An estimate of the stratospheric input to the troposphere during TOPSE using ^{7}Be measurements and model simulations, *J. Geophys. Res.*, *108*, doi:10.1029/2001JD001428, in press, 2003.

Anderson, B. E., G. L. Gregory, J. D. W. Barrick, J. E. Collins Jr., G. W. Sachse, M. C. Shipham, and C. H. Hudgins, Summertime tropospheric ozone distributions over central and eastern Canada, *J. Geophys. Res.*, *99*, 1781–1792, 1994.

Atkinson, R., Gas-phase tropospheric chemistry of organic compounds, *J. Phys. Chem. Ref. Data Monogr.*, *2*, 1994.

Atkinson, R., D. L. Baulch, R. A. Cox, R. F. Hampson Jr., J. A. Kerr, and J. Troe, Evaluated kinetic and photochemical data for atmospheric chemistry, supplement IV, *J. Phys. Chem. Ref. Data*, *21*, 1125–1444, 1992.

Blake, N. J., D. R. Blake, B. C. Sive, A. S. Katzenstein, S. M. Meinardi, O. W. Wingenter, E. L. Atlas, F. Flocke, B. A. Ridley, and F. S. Rowland, The seasonal evolution of NMHCs and light alkyl nitrates at mid to high northern latitudes during TOPSE, *J. Geophys. Res.*, *108*, doi:10.1029/2001JD001467, in press, 2003.

Browell, E. V., et al., Ozone, aerosol, potential vorticity, and trace gas trends observed at high latitudes over North America from February to May 2000, *J. Geophys. Res.*, *108*, doi:10.1029/2001JD001390, in press, 2003.

Brune, W. H., P. S. Stevens, and J. H. Mather, Measuring OH and HO_2 in troposphere by laser-induced fluorescence at low pressure, *J. Atmos. Sci.*, *52*, 3328–3336, 1995.

Brune, W. H., et al., Airborne in-situ OH and HO_2 observations in the cloud-free troposphere and lower stratosphere during SUCCESS, *Geophys. Res. Lett.*, *25*, 1701–1704, 1998.

Brune, W. H., et al., OH and HO_2 chemistry in the North Atlantic free troposphere, *Geophys. Res. Lett.*, *26*, 3077–3080, 1999.

Burkert, J., D. Stöbener, M. Weissenmayer, D. Perner, J. P. Burrows, T. Behmann, and M. D. Andrés-Hernández, Measurements of peroxy radicals in a forested area of Portugal, *Chemosphere, Global Change Sci.*, *3*, 327–338, 2001.

Cadle, R. D., and H. S. Johnston, Chemical reactions in Los Angeles smog, in *Proceedings of the 2nd National Air Pollution Symposium*, pp. 28–34, Stanford Res. Inst., Menlo Park, Calif., 1952.

Calvert, J. G., and W. R. Stockwell, Deviations from the O_3-NO-NO_2 photostationary state in tropospheric chemistry, *Can. J. Chem.*, *61*, 983–992, 1983.

Cantrell, C. A., R. E. Shetter, T. M. Gilpin, J. G. Calvert, F. L. Eisele, and D. J. Tanner, Peroxy radical concentrations measured and calculated from trace gas measurements in the Mauna Loa Observatory Photochemistry Experiment 2, *J. Geophys. Res.*, *101*, 14,653–14,664, 1996a.

Cantrell, C. A., R. E. Shetter, T. M. Gilpin, and J. G. Calvert, Peroxy radicals measured during Mauna Loa Observatory Photochemistry Experiment 2: The data and first analysis, *J. Geophys. Res.*, *101*, 14,643–14,652, 1996b.

Cantrell, C. A., A. Zimmer, and G. S. Tyndall, Absorption cross sections for water vapor from 183 to 193 nm, *Geophys. Res. Lett.*, *24*, 2195–2198, 1997a.

Cantrell, C. A., R. E. Shetter, J. G. Calvert, F. L. Eisele, E. Williams, K. Baumann, W. H. Brune, P. S. Stevens, and J. H. Mather, Peroxy radicals from photostationary state deviations and steady state calculations during the Tropospheric OH Photochemistry Experiment at Idaho Hill, Colorado, 1993, *J. Geophys. Res.*, *102*, 6369–6378, 1997b.

Cantrell, C. A., G. D. Edwards, S. Stephens, L. Mauldin, M. Zondlo, E. Koscuich, and F. Eisele, Steady state free radical budgets and ozone photochemistry during TOPSE, *J. Geophys. Res.*, *108*, doi:10.1029/2002JD002715, in press, 2003.

Carpenter, L. J., S. A. Penkett, J. N. Cape, G. G. McFadyen, K. C. Clemitshaw, and R. A. Burgess, Investigation and evaluation of the NO_x/O_3 photochemical steady state, *Atmos. Environ.*, *32*, 3353–3365, 1998.

Carslaw, N., D. J. Creasey, D. E. Heard, A. C. Lewis, J. B. McQuaid, M. J. Pilling, P. S. Monks, B. J. Bandy, and S. A. Penkett, Modeling OH, HO_2, and RO_2 radicals in the marine boundary layer, 1, Model construction and comparison with field measurements, *J. Geophys. Res.*, *104*, 30,241–30,255, 1999a.

Carslaw, N., P. J. Jacobs, and M. J. Pilling, Modeling OH, HO_2, and RO_2 radicals in the marine boundary layer, 2, Mechanism reduction and uncertainty analysis, *J. Geophys. Res.*, *104*, 30,257–30,273, 1999b.

Cohan, D. S., M. G. Schultz, D. J. Jacob, B. G. Heikes, and D. R. Blake, Convective injection and photochemical decay of peroxides in the tropical upper troposphere: Methyl iodide as a tracer of marine convection, *J. Geophys. Res.*, *104*, 5717–5724, 1999.

Cohen, R. C., et al., Are models of catalytic removal of O_3 by HO_x accurate? Constraints from in situ measurements of the OH to HO_2 ratio, *Geophys. Res. Lett.*, *21*, 2539–2542, 1994.

Crawford, J., et al., Assessment of upper tropospheric HO_x sources over the tropical Pacific based on NASA GTE/PEM data: Net effect on HO_x and other photochemical parameters, *J. Geophys. Res.*, *104*, 16,255–16,273, 1999.

Creasey, D. J., D. E. Heard, and J. D. Lee, OH and HO_2 measurements in a forested region of north-western Greece, *Atmos. Environ.*, *35*, 4713–4724, 2001.

Crutzen, P. J., Ozone production rates in an oxygen-nitrogen oxide atmosphere, *J. Geophys. Res.*, *70*, 7311–7327, 1971.

Crutzen, P. J., and P. H. Zimmermann, The changing photochemistry of the troposphere, *Tellus*, *43AB*, 136–151, 1991.

Crutzen, P. J., M. G. Lawrence, and U. Pöschl, On the background photochemistry of tropospheric ozone, *Tellus*, *51AB*, 123–146, 1999.

DeMore,, W. B., S. P. Sander, D. M. Golden, R. F. Hampson, M. J. Kurylo, C. J. Howard, A. R. Ravishankara, C. E. Kolb, and M. J. Molina, Chemical kinetics and photochemical data for use in stratospheric modeling, evaluation number 12, *JPL Publ. 97-4*, 1997.

Dibb, J. E., R. W. Talbot, E. Scheuer, G. Seid, L. DeBell, B. Lefer, and B. Ridley, Stratospheric influence on the northern North American free troposphere during TOPSE: ^{7}Be as a stratospheric tracer, *J. Geophys. Res.*, *108*, doi:10.1029/2001JD001347, in press, 2003.

Eisele, F. L., D. J. Tanner, C. A. Cantrell, and J. G. Calvert, Measurements and steady state calculations of OH concentrations at Mauna Loa Observatory, *J. Geophys. Res.*, *101*, 14,665–14,679, 1996.

Elrod, M. J., D. L. Ranschaert, and N. J. Schneider, Direct kinetics study of the temperature dependence of the CH_2O branching channel for the $CH_3O_2 + HO_2$ reaction, *Int. J. Chem. Kinet.*, *33*, 363–376, 2001.

Emmons, L. K., et al., The budget of tropospheric ozone during TOPSE from two CTMs, *J. Geophys. Res.*, submitted, 2003.

Fried, A., et al., Tunable diode laser measurements of formaldehyde during the TOPSE 2000 study: Distributions, trends, and model comparisons, *J. Geophys. Res.*, *108*, doi:10.1029/2002JA002208, in press, 2003.

Harder, J. W., A. Fried, S. Sewell, and B. Henry, Comparison of tunable diode laser and long-path ultraviolet/visible spectroscopic measurements of ambient formaldehyde concentrations during the 1993 OH Photochemistry Experiment, *J. Geophys. Res.*, *101*, 6267–6282, 1996.

Hauglustaine, D. A., S. Madronich, B. A. Ridley, J. G. Walega, C. A. Cantrell, and R. E. Shetter, Observed and model-calculated photostationary state at Mauna Loa Observatory during MLOPEX 2, *J. Geophys. Res.*, *101*, 14,681–14,696, 1996.

Hauglustaine, D. A., S. Madronich, B. A. Ridley, S. J. Flocke, C. A. Cantrell, F. L. Eisele, R. E. Shetter, D. J. Tanner, P. Ginoux, and E. L. Atlas, Photochemistry and budget of ozone during the Mauna Loa Photochemistry Experiment (MLOPEX 2), *J. Geophys. Res.*, *104*, 30,275–30,307, 1999.

Heikes, G., B. McCully, X. Zhou, and Y.-N. Lee, Formaldehyde methods comparison in the remote lower troposphere during the Mauna Loa Photochemistry Experiment 2, *J. Geophys. Res.*, *101*, 14,741–14,756, 1996.

Holland, F., U. Aschmutat, M. Hessling, A. Hofzumahaus, and D. H. Ehhalt, Highly time resolved measurements of OH during POPCORN using laser-induced fluorescence spectroscopy, *J. Atmos. Chem.*, *31*, 205–225, 1998.

Hopper, J. F., L. A. Barrie, A. Silis, W. Hart, A. J. Gallant, and H. Dryfhout, Ozone and meteorology during the 1994 Polar Sunrise Experiment, *J. Geophys. Res.*, *103*, 1481–1492, 1998.

Jacob, D. J., Heterogeneous chemistry and tropospheric ozone, *Atmos. Environ.*, *34*, 2131–2159, 2000.

Jaegle, L., et al., Observed OH and HO_2 in the upper troposphere suggest a major source from convective injection of peroxides, *Geophys. Res. Lett.*, *24*, 3181–3184, 1997.

Jaegle, L., D. J. Jacob, W. H. Brune, D. Tan, I. C. Faloona, A. J. Weinheimer, B. A. Ridley, T. L. Campos, and G. W. Sachse, Sources of HO_x and production of ozone in the upper troposphere over the United States, *Geophys. Res. Lett.*, *25*(10), 1709–1712, 1998.

Jaegle, L., et al., Photochemistry of HO_x in the upper troposphere at northern midlatitudes, *J. Geophys. Res.*, *105*(D3), 3877–3892, 2000.

Jaegle, L., D. J. Jacob, W. H. Brune, and P. O. Wennberg, Chemistry of HO_x radicals in the upper troposphere, *Atmos. Environ.*, *35*, 469–490, 2001.

Kanaya, Y., Y. Sudanaga, K. Nakamura, and H. Akimoto, Behavior of OH and HO_2 radicals during the Observations at a Remote Island of Okinawa (ORION99) field campaign, 1, Observation using a laser-induced fluorescence instrument, *J. Geophys. Res.*, *106*, 24,197–24,208, 2001.

Kelly, T. J., D. H. Stedman, J. A. Ritter, and R. B. Harvey, Measurements of oxides of nitrogen and nitric acid in clean air, *J. Geophys. Res.*, *85*, 7417–7425, 1980.

Kim, C.-H., S. M. Kreidenweis, G. Feingold, G. J. Frost, and M. K. Trainer, Modeling cloud effects on hydrogen peroxide and methylhydroperoxide in the marine atmosphere, *J. Geophys. Res.*, *107*, 10.1029/2000JD000285, in press, 2002.

Kleinman, L. I., Ozone process insights from field experiments, 2, Observation-based analysis for ozone production, *Atmos. Environ.*, *34*, 2023–2033, 2000.

Klonecki, A., and H. Levy, Tropospheric chemical ozone tendencies in $CO\text{-}CH_4\text{-}NO_y\text{-}H_2O$ system: Their sensitivity to variations in environmental parameters and their application to global chemistry, *J. Geophys. Res.*, *102*, 21,221–21,238, 1997.

Lanzendorf, E. J., T. F. Hanisco, P. O. Wennberg, R. C. Cohen, R. M. Stimpfle, and J. G. Anderson, Comparing atmospheric $[HO_2]/[OH]$ to modeled $[HO_2]/[OH]$: Identifying discrepancies with reaction rates, *Geophys. Res. Lett.*, *28*, 967–970, 2001.

Lee, M., B. G. Heikes, and D. W. O'Sullivan, Hydrogen peroxide and organic hydroperoxide in the troposphere: A review, *Atmos. Environ.*, *34*, 3475–3494, 2000.

Leighton, P. A., *Photochemistry of Air Pollution*, Academic, San Diego, Calif., 1961.

Lelieveld, J., and P. J. Crutzen, The role of clouds in tropospheric photochemistry, *J. Atmos. Chem.*, *12*, 229–268, 1991.

Lelieveld, J., and P. J. Crutzen, Role of deep cloud convection in the ozone budget of the troposphere, *Science*, *264*, 1759–1761, 1994.

Levy, H., II, Normal atmosphere: Large radical and formaldehyde concentration predicted, *Science*, *173*, 141–143, 1971.

Liu, S. C., et al., A study of the photochemistry and ozone budget during the Mauna Loa Observatory Photochemistry Experiment, *J. Geophys. Res.*, *97*, 10,463–10,471, 1992.

Mari, C., D. J. Jacob, and P. Bechtold, Transport and scavenging of soluble gases in a deep convective cloud, *J. Geophys. Res.*, *105*, 22,255–22,267, 2000.

Mauldin, R. L., III, D. J. Tanner, and F. L. Eisele, Measurements of OH during PEM-Tropics A, *J. Geophys. Res.*, *104*, 5817–5827, 1999.

Mauldin, R. L., III, F. L. Eisele, D. J. Tanner, C. A. Cantrell, E. Kosciuch, J. B. Nowak, G. Chen, D. Davis, B. A. Ridley, and B. Lefer, Measurements of OH aboard the NASA P-3 during PEM-Tropics B, *J. Geophys. Res.*, *106*(D23), doi:10.1029/2000JD900832, 2002.

Mauldin, R. L., III, C. A. Cantrell, M. A. Zondlo, E. Kosciuch, B. A. Ridley, R. Weber, and F. E. Eisele, Measurements of OH, H_2SO_4 and MSA during TOPSE, *J. Geophys. Res.*, submitted, 2003.

Mauzerall, D. L., D. J. Jacob, S.-M. Fan, J. D. Bradshaw, G. L. Gregory, G. W. Sachse, and D. R. Blake, Origin of tropospheric ozone at remote high northern latitudes in summer, *J. Geophys. Res.*, *101*, 4175–4188, 1996.

McElroy, C. T., C. A. McLinden, and J. C. McConnell, Evidence for bromine monoxide in the free troposphere during the Arctic polar sunrise, *Nature*, *397*, 338–341, 1999.

McKeen, S. A., T. Gierczak, J. R. Burkholder, P. O. Wennberg, T. F. Hanisco, E. R. Keim, R.-S. Gao, S. C. Liu, A. R. Ravishankara, and D. W. Fahey, The photochemistry of acetone in the upper troposphere: A source of odd-hydrogen radicals, *Geophys. Res. Lett.*, *24*, 3177–3180, 1997.

Mount, G. H., The measurement of tropospheric OH by long-path absorption, 1.Instrumentation, *J. Geophys. Res.*, *97*, 2427–2444, 1992.

Olson, J. R., et al., Seasonal differences in the photochemistry of the South Pacific: A comparison of observations and model results from PEM-Tropics A and B, *J. Geophys. Res.*, *106*, 32,749–32,766, 2001.

O'Sullivan, D. W., B. Heikes, M. Lee, W. Chang, G. L. Gregory, D. R. Blake, and G. W. Sachse, Distribution of hydrogen peroxide and methylhydroperoxide over the Pacific and South Atlantic Oceans, *J. Geophys. Res.*, *104*, 5635–5646, 1999.

Parrish, D. D., M. Trainer, E. J. Williams, D. W. Fahey, G. Hübler, C. S. Eubank, S. C. Liu, P. C. Murphy, D. L. Albritton, and F. C. Fehsenfeld, Measurements of the $NO_x\text{-}O_3$ photostationary state at Niwot Ridge, Colorado, *J. Geophys. Res.*, *91*, 5361–5370, 1986.

Prather, M. J., and D. J. Jacob, A persistent imbalance in HO_x and NO_x photochemistry of the upper troposphere driven by deep tropical convection, *Geophys. Res. Lett.*, *24*, 3189–3192, 1997.

Press, W. H., S. A. Teukolsky, W. T. Vetterling, and B. P. Flannery, *Numerical Recipes in FORTRAN*, 2nd ed., Cambridge Univ. Press, New York, 1992.

Reiner, T., M. Hanke, F. Arnold, H. Ziereis, H. Schlanger, and W. Junkermann, Aircraft-borne measurements of peroxy radicals by chemical conversion/ion molecule reaction mass spectrometry: Calibration, diagnostics, and results, *J. Geophys. Res.*, *104*, 18,647–18,659, 1999.

Ridley, B. A., S. Madronich, R. B. Chatfield, J. G. Walega, R. E. Shetter, M. A. Carroll, and D. D. Montzka, Measurements and model simulations of the photostationary state during the Mauna Loa Observatory Photochemistry Experiment: Implications for radical concentrations and ozone production and loss rates, *J. Geophys. Res.*, *97*, 10,375–10,388, 1992.

Ridley, B. A., et al., Ozone depletion events observed in the high latitude surface layer during the TOPSE aircraft program, *J. Geophys. Res.*, *108*, doi:10.1029/2001JD001507, in press, 2003.

Ritter, J. A., D. H. Stedman, and T. J. Kelly, Ground level measurements of nitric oxide, nitrogen dioxide and ozone in rural air, in *Nitrogeneous Air Pollutants: Chemical and Biological Implications*, edited by D. Grosjean, Butterworth-Heinemann, Woburn, Mass., 1979.

Roehl, C. M., S. A. Nizkorodov, H. Zhang, G. A. Blake, and P. O. Wennberg, Photodissociation of peroxynitric acid in the near-IR, *J. Phys. Chem.*, in press, 2002.

Roelofs, G.-J., and J. Lelieveld, Distribution and budget of O_3 in the troposphere calculated with a chemistry general circulation model, *J. Geophys. Res.*, *100*, 20,983–20,998, 1995.

Sander, S. P., et al., Chemical kinetics and photochemical data for use in stratospheric modeling, evaluation number 13, *JPL Publ. 00-3*, 2000.

Schultz, M., M. Heitlinger, D. Mihelcic, and A. Volz-Thomas, Calibration source for peroxy radicals with built-in actinometry using H_2O and O_2 photolysis at 185 nm, *J. Geophys. Res.*, *100*, 18,811–18,816, 1995.

Shetter, R. E., and M. Mueller, Photolysis frequency measurements using actinic flux spectroradiometry during the PEM-Tropics mission: Instrumentation description and some results, *J. Geophys. Res.*, *104*, 5647–5662, 1999.

Singh, H. B., D. O'Hara, D. Herlth, W. Sachse, D. R. Blake, J. D. Bradshaw, M. Kanakidou, and P. J. Crutzen, Acetone in the atmosphere: Distribution, sources and sinks, *J. Geophys. Res.*, *99*, 1805–1819, 1994.

Snow, J. A., B. G. Heikes, J. T. Merrill, A. Fried, B. P. Wert, A. J. Wimmers, J. L. Moody, B. Ridley, J. Walega, and C. Cantrell, Winter-spring evolution and variability of HO_x reservoir species, hydrogen peroxide, methyl hydroperoxide and formaldehyde in the northern mid- to high-latitudes, *J. Geophys. Res.*, *107*, doi:10.1029/2002JD002172, in press, 2003.

Staffelbach, T. A., G. L. Kok, B. G. Heikes, B. McCully, G. I. Mackay, D. R. Karecki, and H. I. Schiff, Comparison of hydroperoxide measurements made during the Mauna Loa Observatory Photochemistry Experiment 2, *J. Geophys. Res.*, *101*, 14,729–14,740, 1996.

Stevens, P. S., et al., HO_2/OH and RO_2/HO_2 ratios during the Tropospheric OH Photochemistry Experiment: Measurement and theory, *J. Geophys. Res.*, *102*, 6379–6391, 1997.

Stockwell, W. R., On the $HO_2 + HO_2$ reaction: Its misapplication in atmospheric chemistry models, *J. Geophys. Res.*, *100*, 11,695–11,698, 1995.

Tan, D., et al., HO_x budgets in a deciduous forest: Results from the PROPHET summer 1998 campaign, *J. Geophys. Res.*, *106*, 24,407–24,427, 1998.

Thornton, J. A., P. J. Wooldridge, and R. C. Cohen, Atmospheric NO_2: In situ laser-induced fluorescence detection at parts per trillion mixing ratios, *Anal. Chem.*, *72*, 528–539, 2000.

Tyndall, G. S., R. A. Cox, C. Granier, R. Lesclaux, G. K. Moortgat, M. J. Pilling, A. R. Ravishankara, and T. J. Wallington, Atmospheric chemistry of small organic peroxy radicals, *J. Geophys. Res.*, *106*, 12,157–12,182, 2001.

Wang, C., and R. G. Prinn, On the roles of deep convective clouds in tropospheric chemistry, *J. Geophys. Res.*, *105*, 22,269–22,297, 2000.

Wang, Y., et al., Springtime photochemistry at nornthern mid and high latitudes, *J. Geophys. Res.*, *107*, doi:10.1029/2001JD002227, in press, 2000.

Wennberg, P. O., et al., Removal of stratospheric O_3 by radicals: In situ measurements of OH, HO_2, NO, NO_2, ClO, and BrO, *Science*, *266*, 398–404, 1994.

Wennberg, P. O., et al., Hydrogen radicals, nitrogen radicals, the production of O_3 in the upper troposphere, *Science*, *279*, 49–53, 1998.

Yienger, J. J., A. A. Klonecki, H. Levy II, W. J. Moxim, and G. R. Carmichael, An evaluation of the chemistry's role in the winter-spring ozone maximum found in the northern midlatitude free troposphere, *J. Geophys. Res.*, *104*, 3655–3667, 1999.

Zhang, H., C. M. Roehl, S. P. Sander, and P. O. Wennberg, Intensity of the second and third OH overtones of H_2O_2, HNO_3, and HO_2NO_2, *J. Geophys. Res.*, *105*, 14,593–14,598, 2000.

E. Atlas, T. Campos, C. A. Cantrell M. Coffey, F. Eisele, A. Fried, F. Flocke, S. Hall, J. Hannigan, E. Kosciuch, B. Lefer, L. Mauldin, B. Ridley, R. Shetter, S. Stephens, J. Walega, A. Weinheimer, B. Wert, and M. Zondlo, Atmospheric Chemistry Division, National Center for Atmospheric Research, Boulder, CO 80303, USA. (cantrell@ncar.ucar.edu)

D. Blake, N. Blake, A. Katzenstein, and J. Lopez, University of California-Irvine, Irvine, CA, USA.

E. V. Browell, Atmospheric Sciences, NASA Langley Research Center, MS-401A, Hampton, VA, USA.

J. Dibb, E. Scheuer, G. Seid, and R. Talbot, University of New Hampshire, Durham, NH, USA.

B. Heikes and J. Snow, School of Oceanography, University of Rhode Island, Narragansett, RI, USA.